The potential of ground based arrays of imaging atmospheric Cherenkov telescopes. I. Determination of shower parameters

F.A. Aharonian, W. Hofmann, A.K. Konopelko, H.J. Völk
Max-Planck-Institut für Kernphysik, D-69029 Heidelberg, Germany

The performance of the arrays of imaging atmospheric Cherenkov telescopes (IACTs) for detection of ≥ 100 GeV γ-rays is discussed. The effective detection area of stereoscopic multi-IACT systems is determined essentially by the total geometrical area of the array which may be covered by independent standard ≥ 3 telescope 'cells' with a linear size of about 100 m. We have investigated the characteristics of a quadrangular $100 \times 100\,\mathrm{m}^2$ 'cell' with four '100 GeV' class IACTs in its corners which is recommended as an optimal design for the future IACT arrays. The idea of the 'cell' makes straightforward the study of the characteristics of IACT arrays. The conclusions obtained, concerning in particular the angular and energy resolutions, and the cosmic ray background rejection efficiency, are rather general and do not depend on the specific configuration of the array.

1. Introduction

High-energy gamma-rays carry direct information about relativistic nonthermal processes in astrophysical objects, and it is expected that in the future γ-ray astronomy may play the crucial role in the exploration of violent nonthermal phenomena in the Universe. The recent results of the Energetic Gamma-Ray Experiment Telescope (EGRET) on the Compton GRO are beginning to confirm this prime motivation of γ-ray astronomy. Representatives of different classes of astrophysical sources, in particular quasars, pulsars, supernovae remnants, etc, which were predicted as potential GeV γ-ray emitters, are already in the EGRET source catalogs [1,2]. However the present results of γ-ray astronomy do not yet provide definite answers to many basic questions concerning the origin of the observed radiation. The necessity for new satellite observations in the GeV range with more sensitive γ-ray detectors, in particular for deeper sky surveys, is undisputed. Also, since most of the EGRET sources do not exhibit spectral cutoffs, the extension into the unexplored region beyond 10 GeV is thought to be the second important issue. However, for any practicable effective areas of satellite borne detectors ($S \leq 10\,\mathrm{m}^2$) the very high energy (VHE) region above 100 GeV will remain the domain of ground-based γ-ray detectors. Moreover, it is likely that the ground-based detectors will fill the gap in high energy γ-ray observations from space which is expected for a number of years after the GRO mission.

Various techniques have been applied in the past to detect primary γ-rays by ground-based instruments [3], but at present the IACT technique has proven the most promising approach in VHE γ-ray astronomy (see e.g. [4,5]). Detections of $\geq 10\,\sigma$ DC signals using this technique from four astronomical objects, the Crab Nebula, the PSR B1706-44, and the AGNs Mrk 421, and Mrk 501 (for review, see e.g. [6]) are impressive even by the standards of EGRET.

The further development of the IACT technique over the next few years is likely to occur in two general directions: (a) reduction of the energy threshold of detectors towards the 10 GeV domain using individual large light collectors and, hopefully, high ($\gg 10\%$) quantum efficiency optical detectors, combined with advanced techniques for image analysis, and (b) significant improvement of the CR background rejection efficiency of medium-sized telescopes in the ≥ 100 GeV region and increase of the detection rates using stereoscopic multi-telescope systems (arrays) with total area up to $\approx 1\,\mathrm{km}^2$.

With energy thresholds of future atmospheric Cherenkov detectors going down to 10 GeV, the gap between the energy regions of the satellite and ground-based observations would be eliminated, and the 'horizon' of ground-based γ-ray observations would be extended to cosmological distances beyond redshift $z = 1$. The motivation to operate as near as possible to the EGRET energy region has initiated new activities (see e.g. [7] and references therein) towards low threshold detectors such as the "Solar One" [8], "Super CANGAROO" [9], and "MAGIC" [10] projects. Detection of γ-rays with energies well below 100 GeV requires Cherenkov telescopes, installed preferably at high mountain altitudes ($h \geq 2\,\mathrm{km}$), with very large ($> 10^2\,\mathrm{m}^2$) optical reflectors and, desirably, novel fast detectors for optical radiation with high quantum efficiency. Although very attractive, the promise of detection of $\ll 100\,\mathrm{GeV}$ γ-rays and discrimination of these signals from the heavy backgrounds of different origins still needs justification. Experimental work with the aim of lowering the energy threshold of atmospheric Cherenkov detectors down to 10 GeV has already started. The feasibility of the proposed approaches will hopefully be clarified in the next years.

Equally important and astrophysically interesting as the domain of extremely low energies is the "conventional" IACT regime of a few 100 GeV to a few TeV. Many of the basic questions are best addressed at these energies [11], which also provide a superior signal-to-noise ratio for primary γ-rays from sources with flat spectra. The required improvement in quantity and quality of the data in this domain can only be provided by detectors with enlarged effective detection area compared to conventional IACTs, and improved capability to reconstruct air shower properties, such as the energy, direction, and identity of the primary. IACT *arrays* provide these features.

If one limits the energy region to a relatively "modest" energy threshold around 100 GeV, the predictions of characteristics of individual IACTs and of IACT arrays as well as the issues related to their practical implementation can be formulated with a rather high degree of certainty. It is almost undisputed that in this energy region there is no alternative to the *imaging* technique. At energies around 1 TeV most aspects of this technique are well understood, both experimentally and theoretically, and it is expected that the technique can be effectively extended to the energy region $E \sim 100\,\mathrm{GeV}$. In practice, an energy threshold of 100 GeV can be achieved by so called "10 m" class IACTs with reasonably sized optical reflectors ($S_\mathrm{m} \leq 100\,\mathrm{m}^2$) combined with conventional PMT-based high resolution imaging cameras. Indeed, with a typical $\approx 15\%$ "photon-to-electron" conversion factor (determined essentially by the average quantum efficiency of PMTs as well as by losses of Cherenkov photons in the telescope before reaching the photomultipliers), more than 100 photoelectrons produced in the camera by the Cherenkov light of 100 GeV γ-ray showers would be sufficient not only to trigger the telescope, but also to properly reconstruct the shower images in the Cherenkov light. Monte Carlo calculations, starting with the pionering work of Hillas [12], show that the differences in the Cherenkov light images of γ-ray and CR induced showers permit an effective suppression of CR backgrounds, and thus a significant improvement of detector sensitivities. Measured performance characteristics of existing IACTs and Monte Carlo simulations are in excellent agreement; therefore, the predictions given below - which extrapolate modestly beyond the energy range currently probed - should be highly reliable.

The required further improvement of the IACT technique is possible with the stereoscopic measurement of showers by coupling several imaging telescopes to form a system, or array of telescopes, at the same time enlarging the effective detection area. Currently several groups, in particular HEGRA, Durham, CrAO, Whipple, and Cangaroo/Bigrat, started stereoscopic observations of γ-ray sources with 2 IACTs (for a review see [13]). However, the stereo concept can be fully exploited only with upcoming multi-telescope systems of IACTs equipped with high resolution cameras like HEGRA [14] and Telescope Array [15] operating at energies of γ-rays around 500 GeV, and the proposed VERITAS [16] with an energy threshold around 100 GeV.

In this paper and a companion paper, we develop a vision for the performance and capabilities of a next-generation IACT system, and introduce the concept of IACT *cells* as an efficient means to simulate and extrapolate the properties of such systems. The present paper emphasizes system performance in terms of the quality of reconstruction of shower parameters, and in terms of detection rates. The corresponding γ-ray flux sensitivities will be given in the subsequent paper.

2. Features of IACT arrays

Apart from the obvious advantage of a large effective detection area, IACT arrays, due to their capability of stereoscopic observation of air showers, offer the following advantages over single IACTs:

- reconstruction of the arrival direction of *individual* γ-ray showers with high precision,
- improved energy resolution,
- improved rejection of cosmic-ray showers and other sources of background.

Compared to a single IACT, where the shower inclination is measured rather well in the direction perpendicular to the plane spanned by the telescope axis and the shower impact point, but poorly in the in-plane direction, stereoscopic IACT systems allow determination of the arrival direction of individual γ-ray showers with a typical accuracy $\leq 0.1°$, as will be shown in detail below. This feature allows dramatic suppression of the CR background in the case of point γ-ray sources, and mapping of the source density of extended sources.

The intensity in the images of IACTs is of course governed by the energy (and type) of the primary particle; since the light yield varies with distance to the impact point, there is, however, not a one-to-one correspondence between energy and intensity, and hence the intrinsic energy resolution of a single IACT is relatively poor - of order 40%. For point sources, the distance between the shower image and the source position can be used to estimate the shower impact parameter, resulting in an improved resolution of about 25% to 30%. However, this method loses its power for extended sources; it may also introduce a bias in the energy reconstruction if an extended source is treated as a point source. With stereoscopic IACT systems, the impact point is determined for each event with good precision (less than 10 m), and it will be shown that a 20 % energy resolution can be maintained without any assumptions concerning the source shape or source location.

Apart from the directional information, cosmic-ray rejection in IACTs makes use of the fact that the noticeable differences in the development of γ-ray and proton-induced showers are carried over to their Cherenkov images in the focal plane of the telescopes. Even though the images in different projections are not independent of each other, the images detected by different spatially separated telescopes are only partially correlated and their joint analysis should significantly improve the 'γ/proton' separation power.

Furhermore, determination of the energy and core location of showers on an event-by-event basis helps much to increase the CR rejection efficiency. The mean values of different image parameters depend strongly on the primary energy E_0 and on the distance R to the shower core (impact parameter). Correspondingly, each interval of E_0 and R has its own optimal 'cuts' separating the proton and γ-ray image domains. Lacking precise information on E_0 and R, single-IACT analysis usually applies 'average' cuts, which work effectively only in a certain narrow energy interval. In the case of stereoscopic observations of showers the cuts on image parameters can be optimized in different E_0 and R intervals. Below we show that this *differential* approach leads to a significant improvement of the CR rejection efficiency.

Finally, in a system various sources of background are already suppressed or eliminated at the (hardware) trigger level. The conventional trigger condition of imaging telescopes is to have a signal above some critical threshold q_0 in at least m pixels (typically 2) from a total of n PMTs (hereafter denoted as $m/n \geq q_0$). The threshold q_0 is chosen to limit random coincidences due to night sky background (N.S.B.) to an acceptable level. In a system, in addition a coincidence between local triggers of two or more individual telescopes is requested, virtually eliminating N.S.B. as a source of triggers, and allowing lower thresholds. Triggers caused by local muons

- a major limitation of single IACTs with large mirror area - are no longer a concern.

Already for a single IACT, the trigger condition also enhances the relatively *compact* γ-ray images, where the Cherenkov photons are concentrated within a few pixels, compared to the *larger and diffuse* images of proton-induced showers; the effective energy threshold for cosmic-ray protons is about two to three times higher than for γ-rays. Above a certain threshold energy, a γ-ray within distances up to $\sim$ 100 m from a telescope will trigger the telescope with high (near 100%) probability; additional telescope within the light pool will also trigger effectively. In contrast, the trigger probability for cosmic ray hadrons is typically far below 100%, and the multi-telescope coincidence used to trigger an IACT array will further suppress cosmic-ray backgrounds.

After reaching the maximum possible CR background suppression, at both the trigger and software levels – limited by intrinsic shower fluctuations – a further improvement of the flux sensitivity can be achieved only by increasing the shower detection area. In the case of a single telescope the effective detection area is determined by the radius of the Cherenkov light pool $R \sim 100\,\mathrm{m}$. The effective shower detection area of multi ($\gg 10$) telescope systems is determined essentially by the total geometrical area.

3. Layout of an IACT array

The layout of an IACT array, with parameters such as the mirror area and camera design of the individual telescopes, the number of telescopes, and the arrangement of telescopes and spacing between them, is to some extent governed by the physics goals - in particular the energy threshold - but will always involve compromises in particular related to the cost of the system. In the following, we will concentrate on 'sparse' arrays, where the number of telescopes in the typical Cherenkov light pool is matched to the minimal number required for proper reconstruction of the shower, and where all, or most, of the telescopes in the pool are hence required to trigger in coincidence. The scale for the spacing between telescopes is set by the lateral distribution of Cherenkov light from air showers, as shown in Figs. 1a-1d for γ-ray and proton-induced showers of different primary energies and at different observational levels. The Cherenkov light pool produced by γ-ray primaries has a rather flat lateral distribution with a radial size of approximately $100 \div 140\,\mathrm{m}$. The size of the pool is almost independent of the primary photon energy until $E_0 \leq 1\,\mathrm{TeV}$, at least for the observational level $h \leq 3\,\mathrm{km}$.

Given the need for 3 to 4 views to reconstruct a shower reliably (with only two views, all events on or near the line connecting the telescopes do not provide sufficient stereo angle for a decent reconstruction), this pool size of about 30000 m^2 to 60000 m^2 implies an area per telescope around 8000 m^2 to 20000 m^2, or a spacing around 90 m to 140 m. For an effective identification of γ-ray showers and the proper reconstruction of their parameters it is preferable to have a minimum distance of 50 m between the shower impact point and a telescope; with the spacing given above, this condition is usually fulfilled for the majority of the telescopes triggered by a shower. One notes that for γ-ray primaries, one fixed spacing of telescopes serves a wide dynamical range from 10 GeV to 1 TeV.

On can also imagine arrays where the telescopes are more densely packed, and only a subset of the telescopes in the pool is required to trigger; such a system will provide a slightly lower energy threshold and somewhat improved angular resolution, but it is in general not a very economical solution.

A natural arrangement of the IACTs of a large array is in form of a square or triangular grid. As one might naively expect, simulations show that for a given area density of telescopes, the square grid usually provides slightly better detection rates if a 4-fold coincidence between telescopes is requested, and the triangular grid is provides more 3-fold coincidences. The differences between the two variants are, however, small enough to be negligible for practical purposes. In the following, we will concentrate on a square grid.

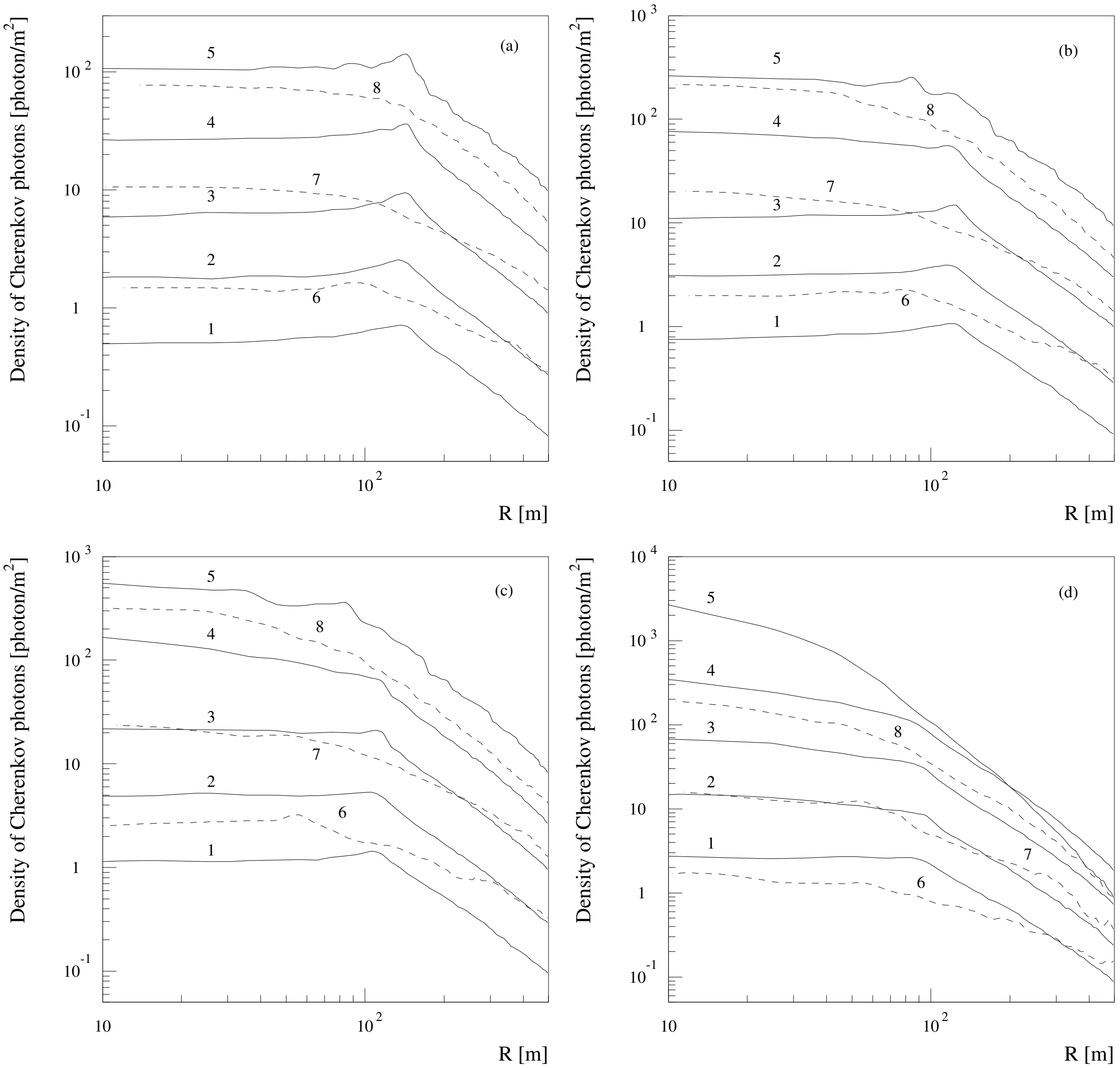

Figure 1. Lateral distribution of the Cherenkov radiation of γ-ray and proton-induced showers at different observational levels: (a) sea level; (b) 2.2 km; (c) 3.5 km; (d) 5.5 km. Solid lines – primary γ-rays of energies 10 GeV (1), 30 GeV (2), 100 GeV (3), 300 GeV (4), 1 TeV (5); dashed lines – primary protons of energies 100 GeV (6), 300 GeV (7), 1 TeV (8).

3.1. Concept of IACT 'cells'

To simulate large IACT arrays efficiently, and to be able to scale the results to arbitrary numbers of IACTs in the system, the 'cell' concept is introduced. A 'cell' is the basic element of the array - a square region with IACTs at the four corners. An array of N times N IACTs will contain $(N-1)^2$ such 'cells'. Air showers with impact points within a given 'cell' will be detected primarily by the four IACTs associated with the 'cell'. Therefore, in the following all simulations are carried out for a single 'cell', considering only showers with impact points inside the 'cell'. The performance of an IACT array with M 'cells' and observation time t is then simply given by the performance of a single 'cell' for observation time Mt; it is therefore straightforward to predict the performance to arbitrary array sizes. In the hardware implementation of a large array, the trigger logic will be arranged locally within a 'cell'. In setting up an array, one will most likely start measurements with a single 'cell' and continuously build up the array; using the 'cell' approach in the analysis allows ready combination of data from different stages.

One notes that the 'cell' approach provides conservative performance figures; in particular at higher energies, telescopes of neighboring 'cells' will provide additional image information and allow improvement of the resolution and background rejection. Furthermore, simulations show that events in a border region of about 1/4 to 1/3 'cell' width around the array also provide useful triggers. This implies in particular that the first 'cell' of an array may provide an effective area equal to about 2 times the 'cell' area, if all events are used.

To illustrate the influence of the size of a quadratic IACT 'cell', Fig. 2 shows the dependence of γ-ray and proton detection rates on the 'cell' size, as derived from a simplified simulation [17]. From this point of view optimal 'cell' sizes range from 100 m to 125 m, depending on the exact trigger condition. One notes the additional suppression of proton showers compared to γ-ray showers for the larger 'cell' sizes. On the other hand, an increased 'cell' size leads to a higher energy threshold. For the detailed simulations presented later, a 'cell' size of 100 m was used.

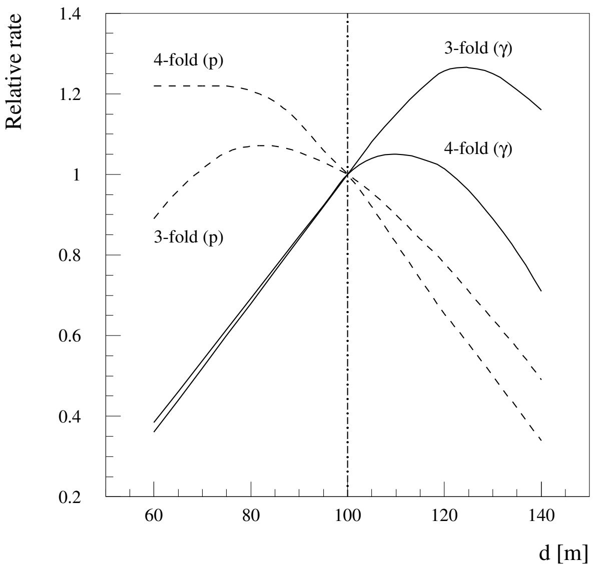

Figure 2. Detection rates of γ-rays and protons within the 'cell', as a function of the 'cell' size, normalized at 100 m 'cell' size. The IACT configuration and trigger conditions are described in Section 3.2.

3.2. Telescope configuration

The telescope energy threshold primarily depends on the geometrical area of the optical reflector $S_{\rm m}$, and on the so called 'photon-to-photoelectron' conversion factor $\chi_{\rm ph\rightarrow e}$, the latter being determined by the quantum efficiency of the light detectors, the mirror reflectivity, and other possible losses of the Cherenkov light on the way from the mirror surface to the light detectors, in particular in the light guides which are normaly placed in front of the PMT array to compensate for the dead space between the photocathodes of PMTs. For conventional aluminized glass mirrors and PMT based imaging cameras the conversion factor $\chi_{\rm ph\rightarrow e}$, averaged over the spectrum of the Cherenkov light of γ-ray showers at the level of observation, is typically between 0.1 and 0.2. It is expected that in future this parameter may be improved, by a factor of a few, by using advanced light detectors with high ($>50\%$) quantum effi-

Table 1
The minimum trigger thresholds q_0 for two different camera designs: (1) 271 pixels, 0.25° pixel size, N.S.B. = 9 ph.e.; (2) 469 pixels, 0.15° pixel size, N.S.B. = 2.2 ph.e..

Camera design:	trigger—master:	1/4	2/4	3/4	4/4
(1)	2/91	q_0 =31	25	23	22
	2/271	q_0 =16	12	11	10
(2)	3/271	q_0 =14	11	10	10
	4/271	q_0 =12	10	9	9

ciency at wavelengths $\lambda \sim 300-400\,$nm.

The number n_0 of photoelectrons produced in the camera by γ-ray showers with core position within 100 m from the telescope, at primary energies around $E_0 \sim 100\,$GeV, is proportional to E_0. For quantitative estimates n_0 may be presented in the form

$$n_0 \approx \rho_0(h) \cdot (E_0/100\,\mathrm{GeV}) \cdot \mathrm{S_m} \cdot \chi_{\mathrm{ph}\to\mathrm{e}}\,, \qquad (1)$$

where the almost radius-independent Cherenkov photon density produced by 100 GeV γ-ray primaries at altitudes $h \simeq 0,\ 2.2,\ 3.5,\ 5.5\,$km a.s.l is $\rho_0(h) \approx 5,\ 10,\ 20,\ 50\,\mathrm{photons/m^2}$, respectively (see Figs. 1a-1d). If one takes into consideration that the minimum number of photoelectrons needed for proper image analysis is estimated to be typically about 100, the γ-ray energy threshold $\approx 100\,$GeV may be achieved by a single IACT located at reasonably high mountain level around 2 km a.s.l., provided that the parameter characterizing the telescope's aperture in respect to the number of photoelectrons, $S_{\mathrm{ph.e.}} = S_{\mathrm{m}} \cdot \chi_{\mathrm{ph}\to\mathrm{e}}$, exceeds $10\,\mathrm{m}^2$.

Note, however, that due to the random triggering of the telescope by the light of N.S.B., this requirement is a necessary but yet not sufficient condition to reach the lowest possible energy threshold determined only by the statistics of photoelectrons. Actually, the energy threshold is determined essentially by the suppression efficiency of the N.S.B. The trigger criterion of the IACT technique is based on the condition to have a signal in at least m (from the total n) pixels above a certain threshold q_0 (in units of photoelectrons). Effective suppression of the N.S.B. at the hardware level can be provided requiring several PMT pixels in coincidence, but obviously the size of the γ-ray image sets a stringent limit to the maximal number of coincident pixels. This implies that a camera with pixel size noticeably less than the γ-ray image size would have a certain advantage. For example, while for relatively economical cameras with pixel size $\approx 0.25°$ the 2-fold coincidence trigger condition ($m = 2$) does not reduce the detection efficiency of γ-rays, the 4-fold coincidence eliminates almost 50% of γ-ray showers [18]. The 4-fold coincidence requires a pixel size $\sim 0.1°$. However, such a pixel size increases the cost of the camera dramatically, without a corresponding improvement of the image quality [19], at least in the currently used second-moment approach for the image analysis. In the case of the quadrangular $100 \times 100\,\mathrm{m}^2$ IACT 'cell' the disadvantage of cameras with relatively large (e.g. 0.25°) pixel size can be compensated, to a large extent, by the requirement of simultaneous detection of showers by 3 or 4 IACTs working with a *local* 2-fold pixel coincidence trigger condition.

The value of the trigger threshold q_0 for a given single telescope is determined by the mean number of photoelectrons n_{b} produced by N.S.B. photons during the time of the trigger gate ($\sim 10\,$ns). To estimate q_0 for the 'cell' of IACTs with $S_{\mathrm{ph.e.}} = 10\,\mathrm{m}^2$ we scale the value $n_{\mathrm{b}} \approx 1$ ph.-e. measured for the HEGRA imaging telescope CT-3 with aperture $S_{\mathrm{ph.e.}} \approx 1.2\,\mathrm{m}^2$ and 271-channel camera with pixel size 0.25° [20]. The trigger thresholds q_0 calculated for different local trigger ($m/n \geq q_0$) and IACTs master ($i/4$) modes of operation of the 'cell' are presented in Table 1. In particular, in the case of the 3-fold IACT coincidence (3/4), the trigger threshold may be reduced to $q_0 \approx 20$ ph.-e and $q_0 \approx 10$ ph.-e for cameras with pixel sizes 0.25° and 0.15°, respectively.

The second principal parameter of the camera

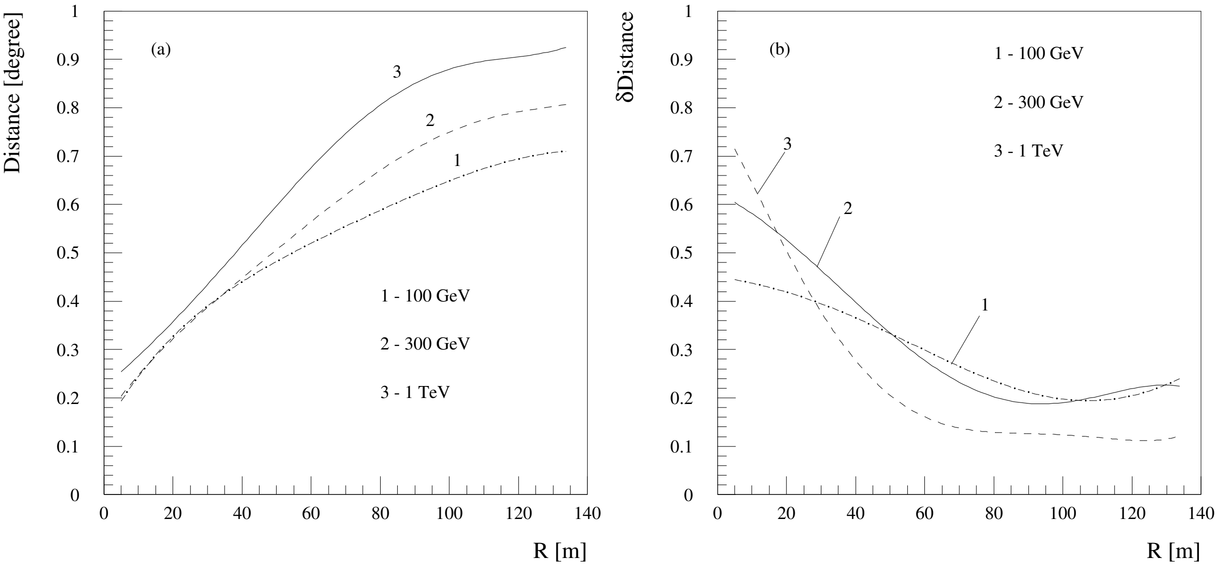

Figure 3. Average angular distance from the centroid of the γ-ray shower image to the center of camera (**D**istance parameter) (a), and its fluctuations δ **D**istance (b) as a function of the impact parameter.

is the field of view (FoV) Ψ. The detection area for γ-rays from a point source increases approximately $\propto \Psi^2$ up to $\Psi \approx 3°$, where Ψ implies the full opening angle of the camera. In principle, $\Psi = 3°$ allows the effective detection of those air showers with direction parallel to the telescope axis, up to impact distances to 140 m. Detection of γ-ray showers beyond 140 m is typically limited by statistics of Cherenkov photons. Therefore, $\Psi \approx 3°$ seems to be the optimal trigger zone. However, in the case of IACTs, the actual field of view of the camera should be larger (by $\geq 1°$) than the the inner $\approx 3°$ acceptance region, where the hardware trigger is organized. Otherwise the limited FoV distorts the shower images, especially those detected at distances $R \sim 100$ m from the telescope; the image centroids of such distant showers are strongly shifted in the focal plane from the center of the camera by $\sim 0.5 - 1°$ (see Fig. 3). Also, cameras with $\geq 3°$ FoV have an obvious advantage in the case of the targets of observations with significant (e.g. $\gg 0.1°$) positional uncertainties, like many EGRET and BATSE sources. And finally, a relatively large FoV of about $5°$ is needed for effective detection of γ-rays from moderately extended sources with angular size $\sim 1°$.

3.3. Monte Carlo simulations for the IACT 'cell'

In this paper we discuss the characteristics of the 'cell' of IACTs having aperture $S_{\rm ph.e.} = S_{\rm m}\chi = 10\,{\rm m}^2$, equipped with high resolution cameras with pixel size $0.25°$ and FoV=$4.75°$, although in some cases we will discuss a $0.15°$ pixel size camera as well. Note that the first configuration corresponds to the 271-pixel cameras currently used in the HEGRA system of 5 IACTs [20]. For the typical value of the 'photon-to-photoelectron' conversion factor around 15% the required aperture $S_{\rm ph.e.} = 10\,{\rm m}^2$ corresponds approximately to a 10 m diameter mirror such as the reflector used in the Whipple IACT [21]. Importantly, for such reflector which may be composed from small $\leq 0.5\,{\rm m}^2$ spherical mirrors, the aberration effects can be effectively overcome [22]. We also suppose that the tracking accuracy and the angular resolution of the composed mirror are essentially better than the pixel size of $0.25°$, both parameters being already achieved in the HEGRA IACTs [20]. Also, in the calculations for

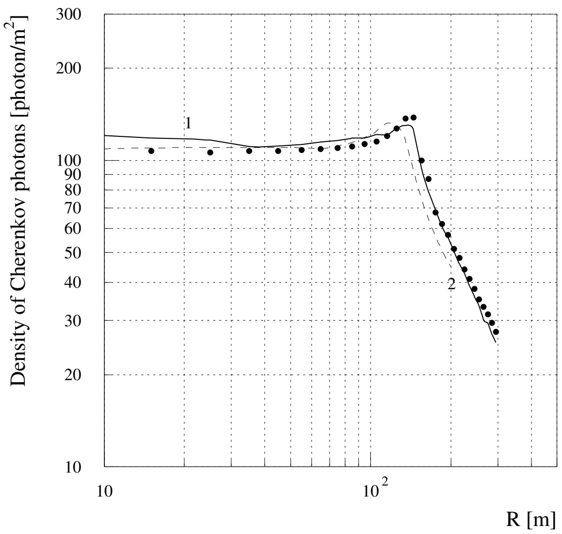

Figure 4. The lateral distribution of the Cherenkov light produced by 1 TeV vertical γ-ray shower at sea level (wavelength range 0.3-0.6 μm) calculated by Hillas A.M. [26] (curve 1) and Sinha [25] (curve 2); dots correspond to our simulations.

the spectral responses of different components of the telescope to the Cherenkov light (i.e. PMT quantum efficiency, mirror reflectivity, etc.) we have used, for definiteness, the averaged characteristics measured for the HEGRA IACTs [20]. Finally, we assume that the telescopes are located at 2.2 km a.s.l.

For simulations of the Cherenkov radiation of air showers at TeV energies the Monte Carlo code described in [23] has been used. The sampling of the electromagnetic cascade development includes the following basic processes: bremsstrahlung, ionization energy losses and Coulomb scattering for charged particles, and pair production and Compton scattering for γ-rays. The data on scattering and absorption of the Cherenkov light in the atmosphere as well as the model of the atmospheric scale height were taken from [24].

In Fig. 4 we compare the lateral distribution of the Cherenkov light photons from 1 TeV γ-ray - induced showers at sea level calculated using this code with analogous recent calculations done by Sinha [25] and Hillas [26].

The simulation of the hadron component of the extensive air shower induced by a primary protons is based on accelerator data. In particular, the total inelastic hadron cross-sections used in the simulation code are taken from [27]. The transverse momenta of the hadrons are determined according to the data from [28]. The inclusive energy spectra of secondaries are taken from [29]. To simulate air showers from primary nuclei, the projectile nucleus is assumed to fragment into independent nucleons. The fragmentation of the colliding nuclei proceeds in accordance with the probability coefficients for the different fragmentation channels obtained by extrapolation of the accelerator data to the multi-TeV energy region. Recently, we have compared the calculations of the hadronic cascade development with the relevant results obtained by the CORSIKA code [30], and found quite satisfactory agreement [31].

The Monte Carlo data include simulated air showers from primary γ-rays, protons and nuclei (of the He, CNO, Si, and Fe groups) in the energy region from 10 GeV to 10 TeV, and for the zenith angles $\theta = 0°, 30°, 45°$. Here we present only the results for vertical showers which are representative for zenith angles up to $\theta = 30°$.

4. Detection efficiencies

There are two basic parameters of a single IACT, the energy threshold and the effective collection area, which determine the statistics of the detected showers. For the given configuration of the telescope, these parameters depend only on the trigger condition, in particular on the pixel trigger threshold q_0.

The effective collection areas for of a single IACT are governed by the lateral and angular distribution of the Cherenkov light. For γ-rays from a point source

$$S_\gamma(E) = 2\pi \int_0^\infty P_\gamma(E,r)\; r dr \tag{2}$$

where $P = P_\gamma(E,r)$ is the detection probability for a γ-ray shower induced by a primary photon with energy E and impact parameter r.

For the isotropic CR background the detection probability $P_{\rm CR}(E,r,\theta)$ depends also on the angle θ between the direction of the primary particle and the axis of the telescope. Thus the effective area integrated over the solid angle of the trigger 'zone' in the camera Ω_t is equal to

$$S_{\rm CR}(E) = 2\pi \int\limits_{\Omega_t} \int\limits_{o}^{\infty} P_{\rm CR}(E,r,\theta)\ rdr\ d\Omega \qquad (3)$$

Note that the detection areas for different species of CRs differ significantly [31].

The detection efficiency of γ-rays by a single IACT at energies above (by a factor of 2) the *effective energy threshold*, the latter being determined as the energy at which the γ-ray detection rate reaches its maximum [32], is almost 100% provided that the telescope is located within the Cherenkov light pool. Thus at high energies the collection area is determined essentially by the effective radius of the light pool, i.e. $S_\gamma \approx \pi R_{\rm eff}^2$, which exceeds by a factor of a few the geometrical area of the chosen IACT 'cell', $S_0 = 10^8\,{\rm cm}^2$. However, in multi-'cell' IACT arrays with the 'cell' linear size comparable with the radius of the disk of the Cherenkov light pool, the loss in area becomes rather negligible, especially for arrays with number of 'cells' $\gg 10$. The ability of stereoscopic measurements by several telescopes to define the shower core position at the observation level $\mathbf{r} = (x,y)$ with an accuracy $\leq 20\,$m (see below), allows one to decompose the statistics of detected showers into the subgroups of events detected by individual 'cells'. Thus, for the given geometrical area of the 'cell' S_0 the effective detection areas of the IACT array consisting of n 'cells' are reduced to

$$\begin{aligned} S_\gamma(E) &= n \cdot S_0 \cdot \varepsilon_\gamma(E) \\ S_{\rm CR}(E) &= n \cdot S_0 \cdot \varepsilon_{\rm CR}(E) \qquad (4) \end{aligned}$$

where $\varepsilon_\gamma(E)$ and $\varepsilon_{\rm CR}(E)$ are the detection efficiences of γ-ray and CR-induced showers with core positions, averaged over the area of the 'cell' and, in the case of CRs, also over the solid angle of the trigger 'zone'. The detection efficiences for CR protons and γ-rays from a point source by the IACT 'cell' for different IACT master criteria '$i/4$' (i=2,3,4 telescopes out of four, triggered in coincidence) and for the local trigger condition in each IACT '$2/91 \geq q_0$' (2 out of the central 91 pixels above q_0) are presented in Fig. 5a. Note that all curves shown are calculated for $q_0 = 25\,$ph.-e. which, in fact, corresponds to the minimum trigger threshold for the master mode 'two telescope out of four in coincidence' (i.e. $i = 2$). For the master requiring four telescopes in coincidence the trigger threshold q_0 may be reduced by additional $20-30\%$ (see Table 1). However, since the exact value of q_0 is determined, in addition to the N.S.B., by some other factors like electronic noise in photomultipliers, here we use a rather conservative value $q_0 = 25\,$ph.-e. for all master modes. The dependence of the shower detection efficiency on the trigger threshold q_0 for the 4-fold IACT coincidence master mode is shown in Fig. 5b.

The trigger criterion '$m/n \geq q_0$' used in IACTs effectively suppresses not only the N.S.B., but also the background caused by CR induced showers having diffuse Cherenkov images in the focal plane. Meanwhile, it sustains a high detection probability of *compact* γ-ray images, where the Cherenkov photons are concentrated in few pixels. Furthermore, the master condition '$i/4$' with $i \geq 2$ provides an additional suppression of the CR background at the hardware level, but does not significantly affect the γ-ray signals. Indeed, due to flat lateral distribution of the Cherenkov light pool produced by γ-rays, the requirement of detection of a shower by ≥ 2 telescopes, at different distances from the shower core does not reduce the number of detected γ-ray showers crossing the 'cell' surface, but works against proton-induced showers the Cherenkov light density has a maximum near the shower core, and falls down at large distances from the core (see Figs. 1a-1d). Moreover, since the position of the Cherenkov images from the isotropic CR showers is determined by the inclination angles to the axis of the telescope and by the distance to the shower core, the probability that the Cherenkov image of the shower will appear outside the field of view of at least one telescope

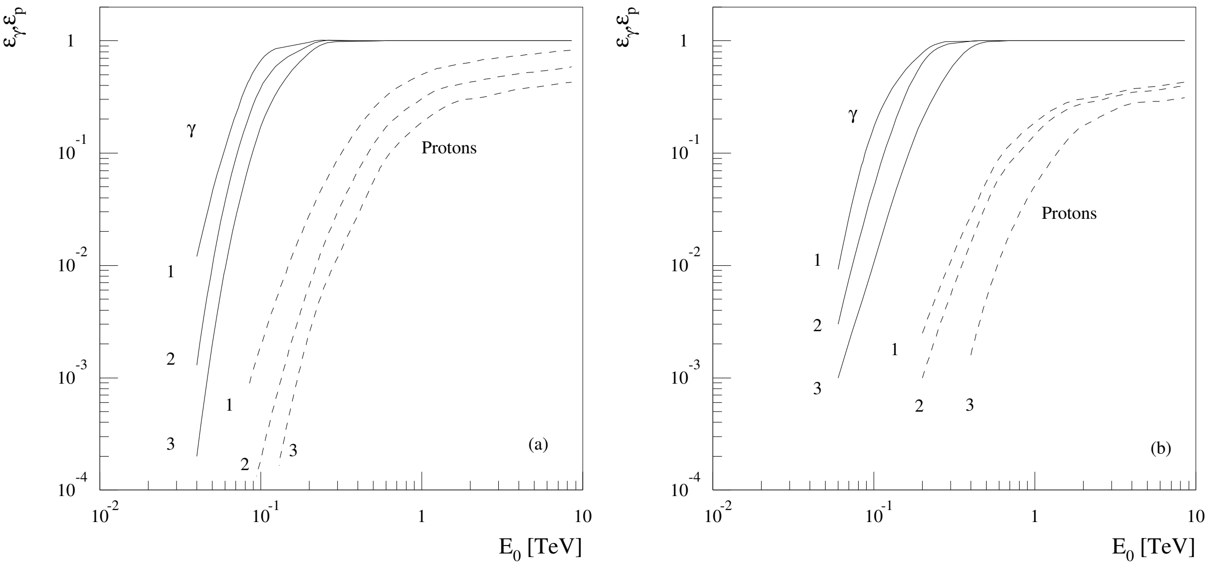

Figure 5. Detection efficiencies of $\gamma-$ray and proton-induced showers by the '100 m $\times$ 100 m' IACT 'cell' for (a) different system master modes (curve 1 - 2/4, curve 2 - 3/4, curve 3 - 4/4; trigger for each IACT 2/91>25 ph.e.) and (b) for different trigger thresholds q_0 (curve 1 - 25 ph.e., curve 2 - 30 ph.e., curve 3 - 50 ph.e.; 4-fold IACT coincidence (4/4) master mode)

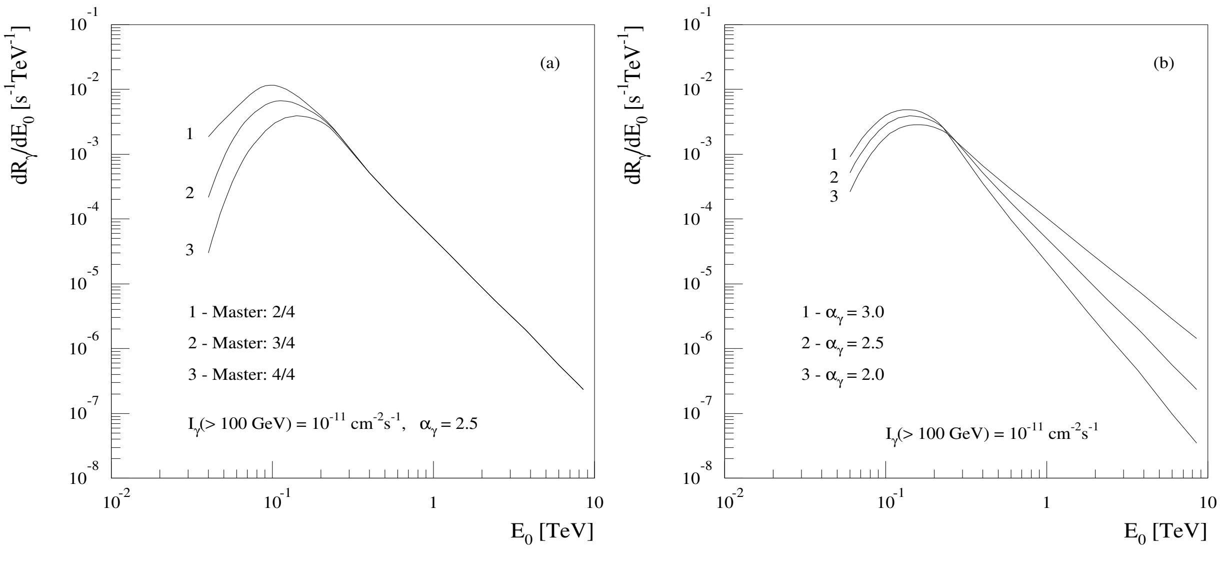

Figure 6. The differential detection rates of γ-ray fluxes given by Eqs.(5) and (6) by the IACT 'cell' for (a) different master modes, and (b) different spectral indices (master mode: 4/4). The camera configuration: 271-channels with 0.25° pixel size; the trigger condition - 2/91>25 ph.e. for each IACT.

Table 2
The detection rates of γ-ray and CR- induced showers [Hz] for the 'cell' of IACTs for different master modes: 2/4, 3/4, 4/4, and for two different configurations of the camera: (1) 271 pixels, 0.25° pixel size, trigger 2/91>25 ph.e.; (2) 469 pixels, 0.15° pixel size, trigger 4/271>10 ph.e. The power-law γ-ray spectra with flux normalization given by Eqs. (5) and (6) are assumed

Camera:	Primary:	Index:	2/4	3/4	4/4
		$\alpha_\gamma = 2.0$	1.24x10^{-3}	1.05x10^{-3}	8.84x10^{-4}
(1)	γ	$\alpha_\gamma = 2.5$	1.47x10^{-3}	1.13x10^{-3}	8.90x10^{-4}
		$\alpha_\gamma = 3.0$	1.82x10^{-3}	1.23x10^{-3}	9.09x10^{-4}
	CR		23.6	10.1	5.3
	e		0.35	0.16	0.07
	σ_0	$\alpha_\gamma = 2.5$	0.018	0.021	0.023
		$\alpha_\gamma = 2.0$	1.30x10^{-3}	1.11x10^{-3}	9.32x10^{-4}
(2)	γ	$\alpha_\gamma = 2.5$	1.56x10^{-3}	1.24x10^{-3}	9.65x10^{-4}
		$\alpha_\gamma = 3.0$	1.92x10^{-3}	1.41x10^{-3}	1.02x10^{-3}
	CR		6.94	2.61	1.15

is rather high; this leads to further suppression of the CR background.

As shown in Fig. 5b, at energies above 200 GeV the detection efficiency of γ-ray showers becomes nearby 100% even for the master which requires the shower detection simultaneously by all four telescopes of the 'cell'. At lower energies the detection efficiency decreases. Still, non-negligible statistics of detected γ-rays may be expected even at energies below 100 GeV, in particular in the case of power-law spectra of γ-radiation. The effective dynamical region of the 'cell', for the given primary spectrum, is characterized by the detection rate of primaries with mean energy E in the interval $\Delta E \approx E$, i.e. by the function $E \times (dR_\gamma/dE)$, where $dR_\gamma/dE = S_\gamma(E) \times dF_\gamma/dE$ is the so-called differential detection rate. Below we will discuss differential power-law spectra of γ-rays

$$\frac{dF_\gamma}{dE} = A \cdot E^{-\alpha_\gamma} \tag{5}$$

with the flux normalization

$$F_\gamma(\geq 100\,\mathrm{GeV}) = 10^{-11}\,\mathrm{cm}^{-2}\mathrm{s}^{-1}\,. \tag{6}$$

Detection rates of γ-rays with spectral index $\alpha_\gamma = 2.5$ by the 'cell' in different master modes are shown in Fig. 6a. The energy at which the detection rate reaches its maximum shifts from 100 GeV at a 2-fold IACT coincidence to 150 GeV

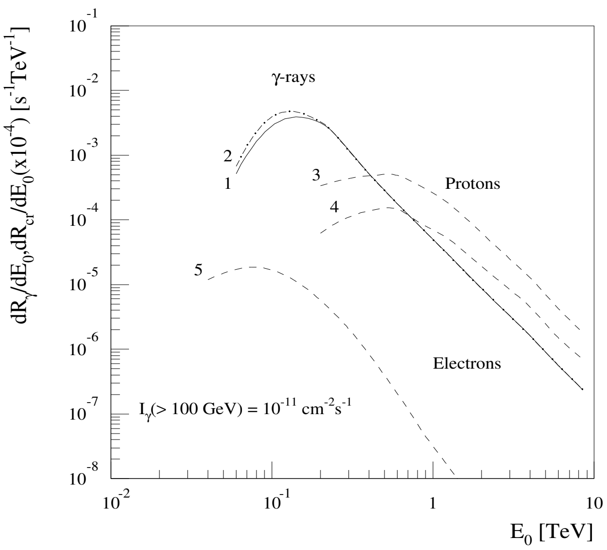

Figure 7. Differential detection rates of γ-rays, CR protons and electrons for the system master mode 4/4. All curves except 2 and 4 are calculated for 0.25° pixel camera (trigger threshold $q_0 = 25$ ph.e.), and curves 2 and 4 are calculated for 0.15° camera ($q_0 = 15$ ph.e.).

for 4-fold IACT coincidence. Note that the maximum of the γ-ray detection rate does not depend much on the spectral index of the primary radiation for a given master mode (see Fig. 6b). In Fig. 7 we show the detection rates of γ-rays, CR protons and electrons by the 'cell' in the IACT master mode 4/4 for two different camera designs: (1) a 217-channel camera with pixel size 0.25° and (2) a 469-channel camera with pixel size 0.15°. It should be noted that for the given mirror aperture $S_{\rm ph.e.}$ smaller pixel size reduces the noise caused by N.S.B., and correspondingly results in lower trigger threshold q_0.

Note that the detection rate of the CR background depends on the CR chemical composition. For the standard CR composition the CR nuclei contribute $\approx 1/3$ to the detection rate of IACTs [31]. Thus, uncertainties in the chemical composition results in non-negligible uncertainties in the CR background rate. However, owing to the very broad shape of images CR nuclei-induced showers, the CR background caused by primary nuclei is automatically removed with almost 100% efficiency when the cuts for γ-ray image shape are applied (see below). Therefore, in Fig. 7 we show only detection rates calculated for the CR proton flux which may be presented in the form (see e.g. [33])

$$\frac{dF_{\rm p}}{dEd\Omega} \approx 1.1 \cdot 10^{-5} E^{-2.75}\, \rm cm^{-2} s^{-1} sr^{-1} TeV^{-1} \quad (7)$$

It is evident from Fig 7 that although the use of a higher resolution camera leads only a slight increase of the γ-ray detection rate at low energies, it provides much better rejection of CRs at the hardware level. However this advantage of the small-pixel camera actually does not imply a significant improvement of the signal-to-noise-ratio, since after the effective suppression of the proton-induced showers at the software level (see below), the contribution of the electron induced showers to the CR background dominates at energies around 100 GeV. Indeed, although at energies above 100 GeV the 'e/p' ratio is less than 1%, detection rates of these 2 components are much closer; the trigger and master conditions used for detection of γ-rays are equally favorable to electron induced showers, but they provide effective

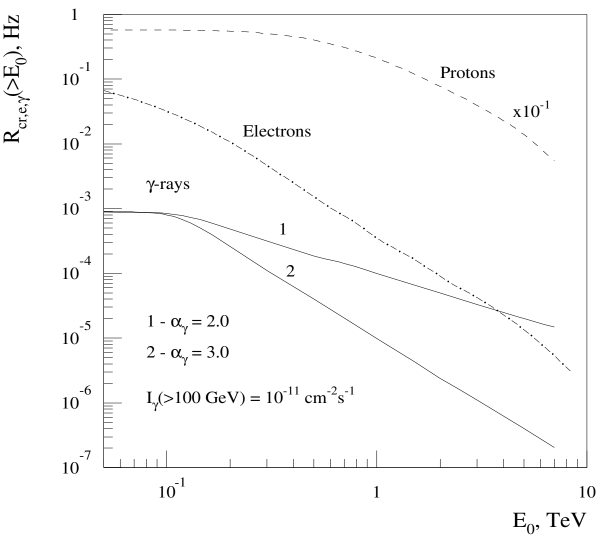

Figure 8. Integral detection rates for plane-parallel flux of $\gamma-$rays and for isotropic proton- and electron-induced showers by the IACT 'cell' in the 4/4 system master mode.

detection of protons only at energies above 1 TeV. In Fig. 7 we present detection rates of CR electrons calculated for the reported differential flux (see e.g. [33])

$$\frac{dF_{\rm e}}{dEd\Omega} \approx 1 \cdot 10^{-8} E^{-3.25}\, \rm cm^{-2} s^{-1} sr^{-1} TeV^{-1} \quad (8)$$

The comparison of integral rates of CR protons and electrons shown in Fig. 8 demonstrates that the electron induced showers become a non-negligible part of the CR background. Moreover, after application of the image software cuts which reject significantly (by a factor of $\geq$ 100; see below) the CR proton-induced showers, the CR electron background becomes the most important limiting factor for sensitivities of low-energy Cherenkov detectors.

The detection rates by the IACT 'cell' of the CR protons and for power-law fluxes of γ-rays from a point source by the IACT 'cell' are shown in Table 2. Note that for the normalization of

γ-ray fluxes at 100 GeV (see Eq.(6)), the γ-ray detection rates depend slightly on the spectral index α_γ. In Table 2 we present also the values of the parameter

$$\sigma_0 = R_\gamma \cdot (R_{\rm p} + R_{\rm e})^{-1/2} \cdot \sqrt{3600\,{\rm s}}\,, \qquad (9)$$

which characterizes the standard deviations above the CR background obtained for 1 h of observations in the tracking mode [1]. Further significant improvement of the γ-ray signal is performed by the software image analysis.

5. Determination of shower parameters

The showers detected by the 'cell' are identified fully by the set $\mathbf{x} = (a,\ E,\ \Omega,\ \mathbf{r})$, where a is the type, E is the energy, Ω is the 3-dimensional vector $(\Omega_x, \Omega_y, \Omega_z)$ of the arrival direction of the primary particle, and $\mathbf{r}$=(x, y) are the coordinates of the shower core in the plane of the 'cell'.

For an individual shower the data set consists of Cherenkov images registered by n IACTs. In the second-moment approach the images are described by several parameters which determine the position, orientation, shape and brightness of the image in the camera. For example, **W**idth, **L**ength parameters are the rms spread of light along the minor and major axes of the image, respectively; **D**istance is the angular distance from the image centroid to the center of the FoV; **A**lpha is the angle between the major axis of the image and the line connecting the image centroid and and the center of the FoV; **S**ize is the total number of photoelectrons in the image. There are few other useful derivative image parameters, in particular the **A**zwidth parameter which is a very convenient combination of the shape and orientational parameters of the image. For a detailed description of these and other (less effective) second-moment parameters of the Cherenkov light images, see [12,34].

[1] Since the stereoscopic observations allow measurement of the direction of showers, it is always possible, at least for γ-ray point sources, to find out a relevant OFF (background) region at a distance $\sim 1^\circ$ from the γ-ray source, operating the IACTs only in the tracking mode, i.e. keeping the axes of telescopes continually in the source direction.

5.1. Determination of arrival directions of primaries

For a single IACT the orientational parameter **A**lpha contains a certain information about the showers arriving from directions close to the axis of the telescope. However, this parameter, reproducing the orientation of the shower core only in one projection, does not allow measurement of the real direction of *individual* events. Thus, a single IACT can be only conditionally called a telescope in the classical meaning of this word. Determination of the arrival direction of primaries on an *event-by-event* basis is possible only by detecting the shower images by at least two separated IACTs. This is one of the important benefits of the operation of imaging telescopes in the stereoscopic mode.

The orientation of the image in the focal plane of each from two ($k = 1, 2$) triggered telescopes is defined as

$$\begin{aligned} \mathbf{e}^k &= (-cos\beta^k, -sin\beta^k), \\ \beta^k &= arctg(\vartheta_y^k/\vartheta_x^k) \pm \alpha^k \end{aligned} \qquad (10)$$

where the vector $\vartheta^k = (\vartheta_x^k, \vartheta_y^k)$ determines the position of the centroid in the focal plane of k th IACT ($\mid \vartheta \mid \equiv$ **D**istance).

Provided that the focal planes of all IACTs are parallel, i.e. all telescopes are directed to the same point in the sky, for each pair of images detected by n separated IACTs (the number of such pairs being $m = C_n^2$), the intersection of the lines along the image major axes gives the source position $\boldsymbol{\theta}^l$=(θ_x^l, θ_y^l) ($l = 1, m$) in the 'common' focal plane:

$$\begin{aligned} &\theta^l - \vartheta^k = e^k \mid \theta^l - \vartheta^k \mid \\ &\qquad l = 1, m; k = 1, 2 \end{aligned} \qquad (11)$$

The procedure of determination of arrival direction of the primary particle is demonstrated in Fig. 9a. Thus, already one pair of detected images is enough to determine unambiguously the shower direction. In the case of detection of ≥ 2 images, the value of θ_0=$\sum \theta^l/m$ averaged over $m = C_n^2$ pairs significantly improves the accuracy of the reconstruction of the arrival direction. However, obviously the pairs with $\mathbf{e}^i \simeq \mathbf{e}^j$ or $\mathbf{e}^i \simeq -\mathbf{e}^j$ should be excluded from consideration. Also, the

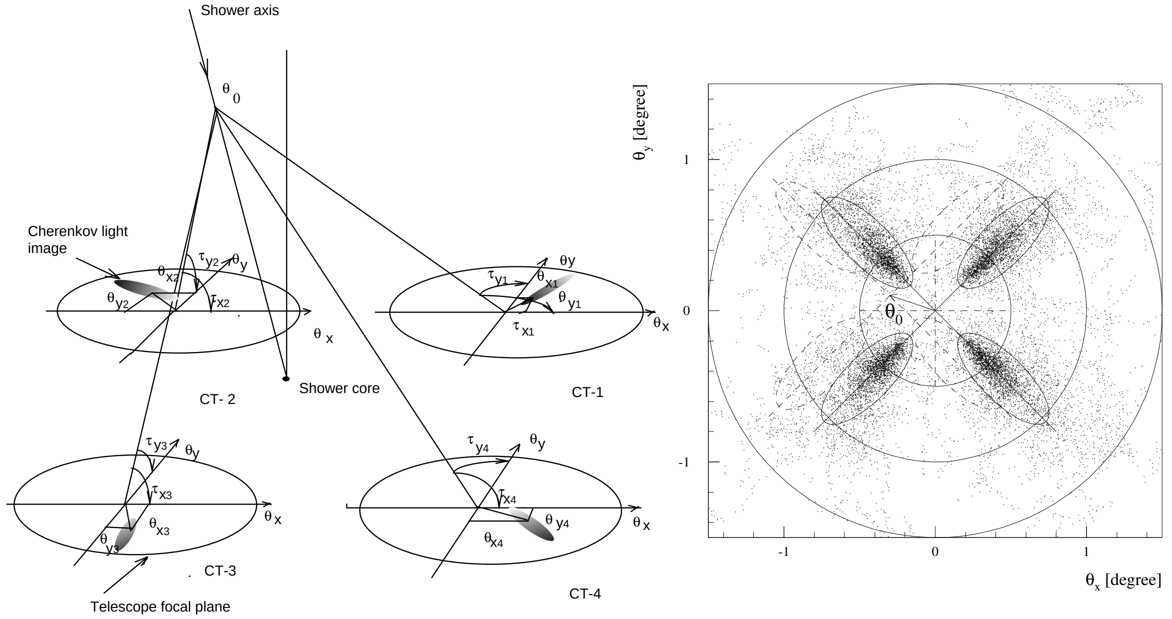

Figure 9. Reconstruction of the arrival direction of showers. The shower impact point on the ground is defined through the angles Θ_x^i, Θ_y^i in the focal plane which determine 3-dimensional angles $\tau_x^i \simeq \Theta_x^i$ and $\tau_y^i \simeq \Theta_y^i$ for $\Theta_{x,y} \simeq sin\Theta_{x,y} << 1$ (left figure). Note that the image **D**istance parameter is defined as $d_i = ((\Theta_x^i)^2 + (\Theta_y^i)^2)^{1/2}$. The camera planes are all parallel but not lying in a common plane. To determine the shower direction the images in all cameras are superposed (right figure). Solid ellipses correspond to shower with direction parallel to the telescope axes, and dotted ellipses correspond to a shower inclined by angle θ.

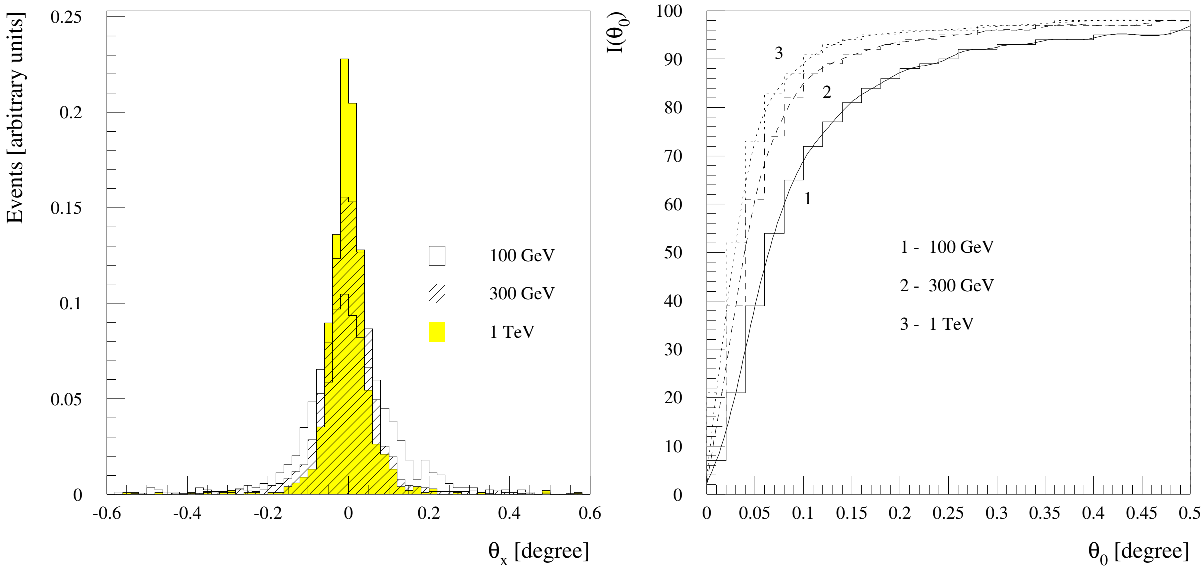

Figure 10. Angular resolution of the IACT ‘cell’ at different energies of primary γ-rays.

images with small angular distances from the center of the camera ϑ and with small **S**ize parameter are best excluded from the summation because of large fluctuations of the orientational **A**lpha parameter.

Note that in the case when the telescope axis is directed to the point source, the center of FoV corresponds to the position of the source. The γ-rays arriving at some angle θ to the telescopes axis (e.g. due to an extended character of the γ-ray source), can be clearly distinguished by the corresponding shift of the coordinates in the camera as far as $\theta \geq 0.1°$ (see Fig. 9b).

One-dimensional angular distributions of monoenergetic γ-rays from a point source with energy E=100 GeV; 300 GeV, and 1 TeV in the telescope focal plane are shown in Fig. 10a. The corresponding probability of the reconstructed source position to be inside the angle $\theta = (\theta_x^2 + \theta_y^2)^{1/2}$ ($\theta = 0°$ corresponds to the direction of the telescope axis) is shown in Fig. 10b. Hereafter we will define the angular resolution $\delta\theta$ of the instrument for individual γ-ray showers by the angle which corresponds to the 68% acceptance of γ-ray events. From Fig. 10b we see that the angular resolution of the 'cell' operating in the '4/4' mode is equal 0.1°, 0.075° and 0.05° for E=100 GeV; 300 GeV, and 1 TeV, respectively.

5.2. Localization of the shower core

For the plane-parallel γ-ray flux the Cherenkov light is seen at large angles if the shower core is far away from the telescope. Correspondingly the Cherenkov images of distant showers are shifted from the center of FoV. Thus, in the case of a γ-ray point source, the position of the image centroid correlates strongly with the shower impact distance. (For the isotropic CR background the Cherenkov images are randomly distributed in the camera, thus there is no correlation between the image centroid position and the distance to the shower core). Therefore, for point γ-ray sources the position of the image centroid in the camera which is characterized by the **D**istance parameter may serve as an informative estimate of the impact distance of the shower induced by a primary photon: $R = f(\mathbf{D}istance)$. However, this procedure contains large systematic

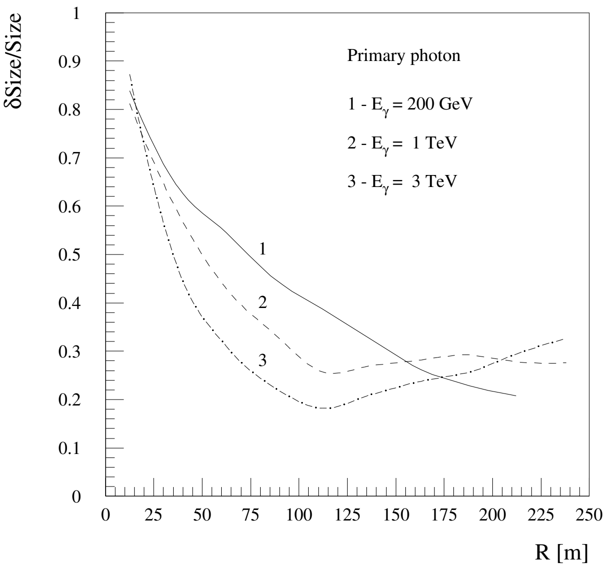

Figure 11. Fluctuations in the total number of photoelectrons produced in the camera by γ-ray showers of different energies.

errors. In particular, the 'R-**D**istance' relation depends actually on the primary photon energy which *a priori* is an unknown parameter, and is different for different primaries. Also, this approach cannot be used for even slightly extended ($\theta \leq 0.5°$) γ-ray sources.

The stereoscopic measurements by at least 2 IACTs make the determination of the position of the shower core straightforward, independent on the type and energy of the primary particle.

Let the telescopes of the 'cell' be distributed on the ground with coordinates $\mathbf{d}^k = (d_x^k, d_y^k, d_z^k)$ (k=1,4), and the optical axes of all IACTs be directed to the source. The orientation of these axes are described by the vector in the *horizontal* coordinate frame

$$\Omega_o = (sin\Theta_z \, cos\varphi, sin\Theta_z \, sin\varphi, cos\Theta_z) \,, \qquad (12)$$

where Θ_z and φ are the zenith and azimuth angles, respectively.

It is convenient to describe the coordinates of the telescopes in the cartesian frame with Z-axis directed along the optical axes of the telescopes and the Y-axis being parallel to the azimuth dir-

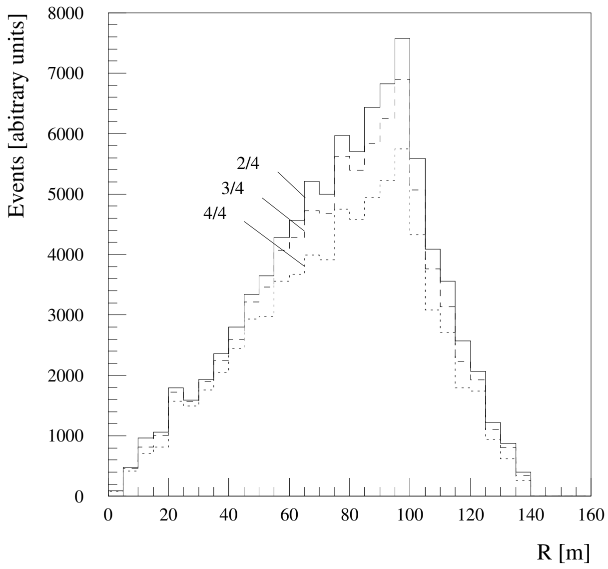

Figure 12. Distribution of the impact distance of the shower core from each of the telescopes for different system master modes.

ection (e.g. [35]),

$$
\begin{aligned}
\tilde{d}_x &= -d_x sin\varphi + d_y cos\varphi \\
\tilde{d}_y &= cos\Theta_z (d_x cos\varphi + d_y sin\varphi) \\
\tilde{d}_z &= d_z + d_y sin\Theta_z \qquad (13)
\end{aligned}
$$

For the (i,j) th pair of the triggered IACTs the impact positions $\mathbf{R}^i = R^i \mathbf{e}^i$, $\mathbf{R}^j = R^j \mathbf{e}^j$ can be found from the following equation:

$$\tilde{\mathbf{d}}^i + \mathbf{R}^i + |\tilde{d}_z^i - \tilde{d}_z^j|\Omega^\circ \simeq \tilde{\mathbf{d}}^j + \mathbf{R}^j \, . \qquad (14)$$

It should be mentioned that the events detected at distances less than 50 m have rather a circular than an elliptical shape. In addition, at small distances to the shower core the fluctuations of the Cherenkov light amplitude (**Size** parameter) are very large (see Fig. 11). Both effects result in large uncertainties in the image orientation. However, for the given configuration of the IACT 'cell', and the requirement to detect showers by all 4 telescopes, the distances of the detected shower to at least 3 telescopes always exceed 50 m. The probability distributions $P_n(< R)$ that the core of the shower, detected by all 4 telescopes of the 'cell', is located at distances less than R from at least two, three, and four telescopes are shown in Fig. 12. It is seen that the number of events with distances less than 75 m from at least two telescopes is rather small which implies that almost all detected events can be stereoscopically reconstructed using high quality images.

The accuracy of determination of the impact distances of primary γ-rays are shown in Fig. 13. The half width at half maximum (HWHM) values at energies E=100 GeV, 300 GeV, and 1 TeV are δR=7 m, 4 m, and 3 m, respectively.

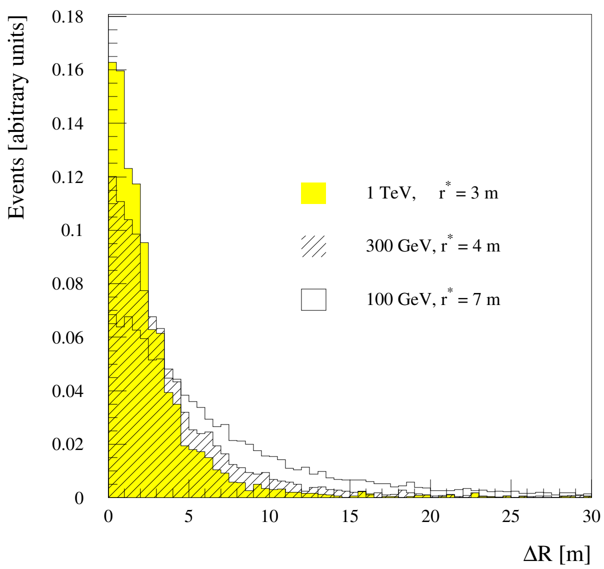

Figure 13. Uncertainties in the reconstructed impact parameter of γ-ray showers of different energies.

5.3. Determination of the shower energy

Determination of the shower core position with an accuracy of ≤ 10 m is quite sufficient, due to the flat lateral distribution of the Cherenkov radiation of γ-ray showers, for the evaluation of the energy of primary γ-rays using the average relation, at the given R, between the image **Size** and the primary energy E. In fact, the accuracy of the energy estimate is determined predomin-

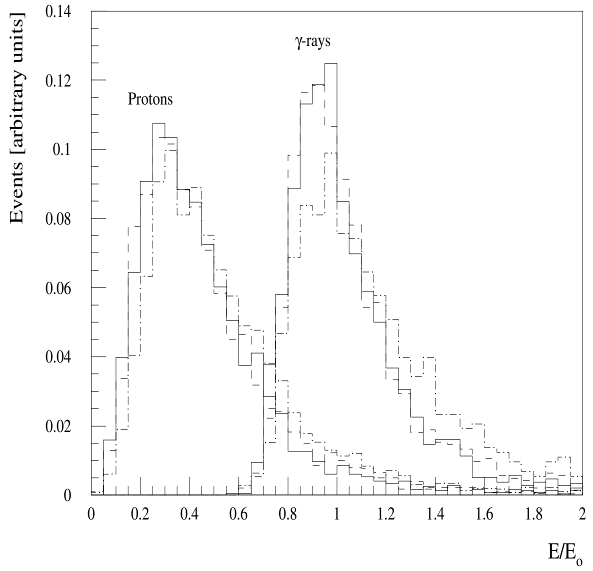

Figure 14. Distribution of the ratio of the reconstructed energy to the primary energy for the γ-ray and proton showers, using the energy determination algorithm tuned for γ-ray showers: $E_0 = 100$ GeV (solid line), 300 GeV (dashed line), 1 TeV (dashed-dotted line).

antly by the fluctuations of the image **S**ize which are rather large ($\geq$ 30%) for close ($R \leq 60\,\mathrm{m}$) as well as very distant ($R \geq 120\,\mathrm{m}$) showers. However, since most of the showers detected by all 4 IACTs are located at distances between 60 m and 120 m (see Fig. 12) from at least two telescopes, the fluctuations appear small enough to provide determination of the energy of γ-ray showers with an accuracy $\leq$ 20% over the dynamical region from 100 GeV to 1 TeV, as it is demonstrated in Fig. 15. Formally, such a claim is correct under the conditions of *background-free* detection of γ-ray signal, i.e. when the number of detected γ-rays exceeds, after the software image analysis, the number of CR-induced showers. The fulfillment of this condition depends on the strength of the γ-ray source, and the CR background suppression efficiency. Given the difference in the Cherenkov light yield between CR-induced and γ-ray -induced showers of the same energy, the algorithm tuned for γ-rays will underestimate the CR energies by a factor of approximately two (compare the lateral distributions of the Cherenkov light from γ-rays and protons shown in Fig. 1a-1d). Therefore, as far as the primaries are not identified on an *event-by-event* basis, CR-induced showers will be sorted into incorrect energy bins. This effect is demonstrated in Fig. 14. However, since the same effect takes place for both 'on-source' and 'off-source' reference samples, the ON-OFF subtraction removes, on average, background events and leaves only γ-rays with properly estimated energies.

6. Separation of gamma-ray- and CR-induced showers

6.1. Suppression of the CR background based on the directional information

The obvious and straightforward method of rejection of the isotropic CR background based on the *directional information* is the selection of the showers within the angle corresponding the angular resolution of the instrument or the presumed source size, whenever is larger. Reconstruction of the shower arrival directions by the IACT 'cell' on an *event-by-event* basis with accuracy $\leq 0.1^\circ$ provides very effective reduction of the CR background contamination in the γ-ray signal from a relatively compact source with angular size significantly less than 1°. In particular, for point γ-ray sources, which in our case implies a source angular size $\psi \leq$ few arcminutes, the contribution of the CR events detected within the trigger region $\approx 3^\circ$ can be reduced by a factor of > 100. Thus the directional information alone already results in a significant enhancement of the signal-to-noise-ratio by a factor of

$$Q^{(\mathrm{dir})} = \kappa_\gamma^{(\mathrm{dir})} / \sqrt{\kappa_{\mathrm{CR}}^{(\mathrm{dir})}} \approx 10\,, \tag{15}$$

where $\kappa_\gamma^{(\mathrm{dir})}$ and $\kappa_{\mathrm{CR}}^{(\mathrm{dir})}$ are the efficiences of the acceptance of γ-rays and CRs within the angle corresponding the angular resolution of the instrument. For comparison, note that in the case of a single telescope the CR background rejection based on the parameter **A**lpha, which contains information about the arrival directions of

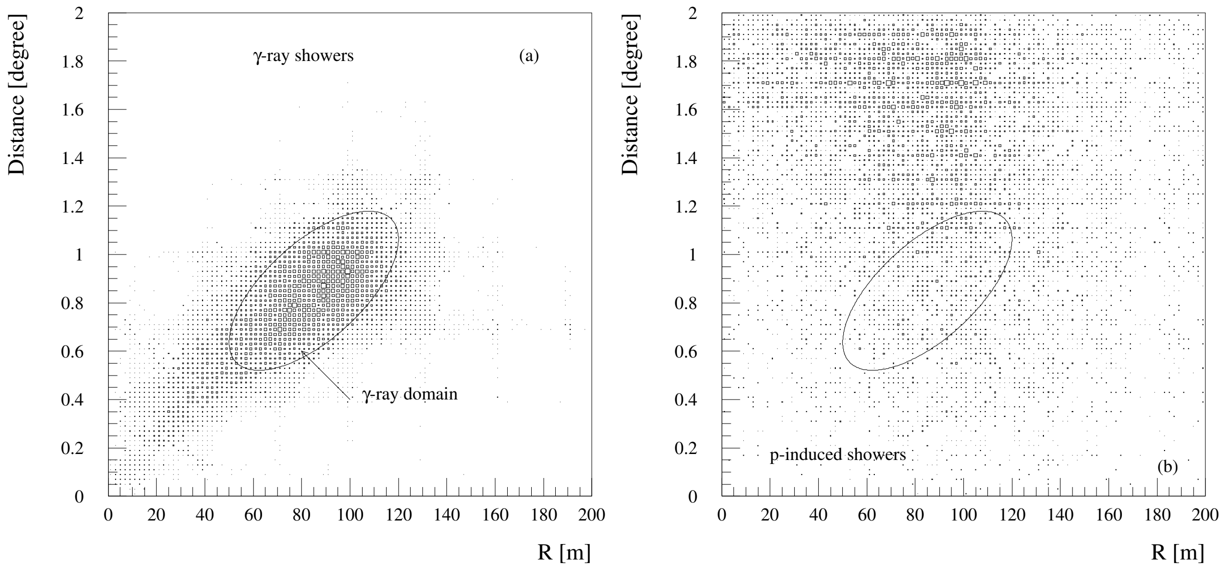

Figure 15. Two-dimensional scatter plot, **D**istance versus R, for (a) γ-ray showers, and (b) CR-induced showers detected by all 4 IACTs of the 'cell'.

air shower in one projection, does not exceed a factor of 10. Indeed, the γ-ray events detected in the direction of the point source are distributed within **A**lpha $\leq 10°$, while the **A**lpha-*distribition* of isotropic CR events is almost constant over the limits from 0° to 90°. Thus, the stereoscopic observations of point γ-ray sources improve the CR background rejection efficiency based on the directional information by a factor of at least 10, if one compares with the observations in the 'mono' mode.

The advantage of the observations in the stereoscopic mode can be demonstrated also by analyzing the *correlations of the image centroid position in the camera with the distance to the shower core.* For the plane-parallel γ-ray flux there is a strong correlation between the **D**istance parameter and the position of the shower core R. The dependence of the **D**istance parameter and its fluctuations on R is shown in Fig. 3. Although the centroid position of the image monotonically increases with R, the **D**istance-distribution of γ-ray showers shows a cutoff at **D**istance$\sim 1°$, even for a large FoV of the camera, which reflects the sharp decrease of the Cherenkov light density beyond 120 m.

The scatter plot **D**istance vs R for γ-ray and CR showers detected by all 4 IACTs of the 'cell' is shown in Fig. 15. Most of the detected γ-ray events are concentrated in a rather compact domain (Fig. 15a). On the other hand the isotropic CR background showers are diffusely distributed in the same plot; they show almost uniform distribution but with some tendency to be concentrated at $R \sim 100$ m and **D**istance$\geq 1°$ (see Fig. 15b). Note that although the maximum distance of the showers to any of 4 IACTs of the 'cell' cannot exceed 140 m, the reconstructed distances for the CR events in Fig. 15b actually extend up to 200 m, the reason for that being large errors in the reconstruction of the inclined CR showers.

The significant difference in the **D**istance-**R** correlations for the γ-ray - and CR-induced showers provides, in the case of γ-ray point sources, a rather high efficiency for suppression of the CR background. Namely, under the condition of 50% acceptance of γ-ray events, the rejection factor of CR showers by the IACT 'cell' can be reached ≈ 200, which results in the sig-

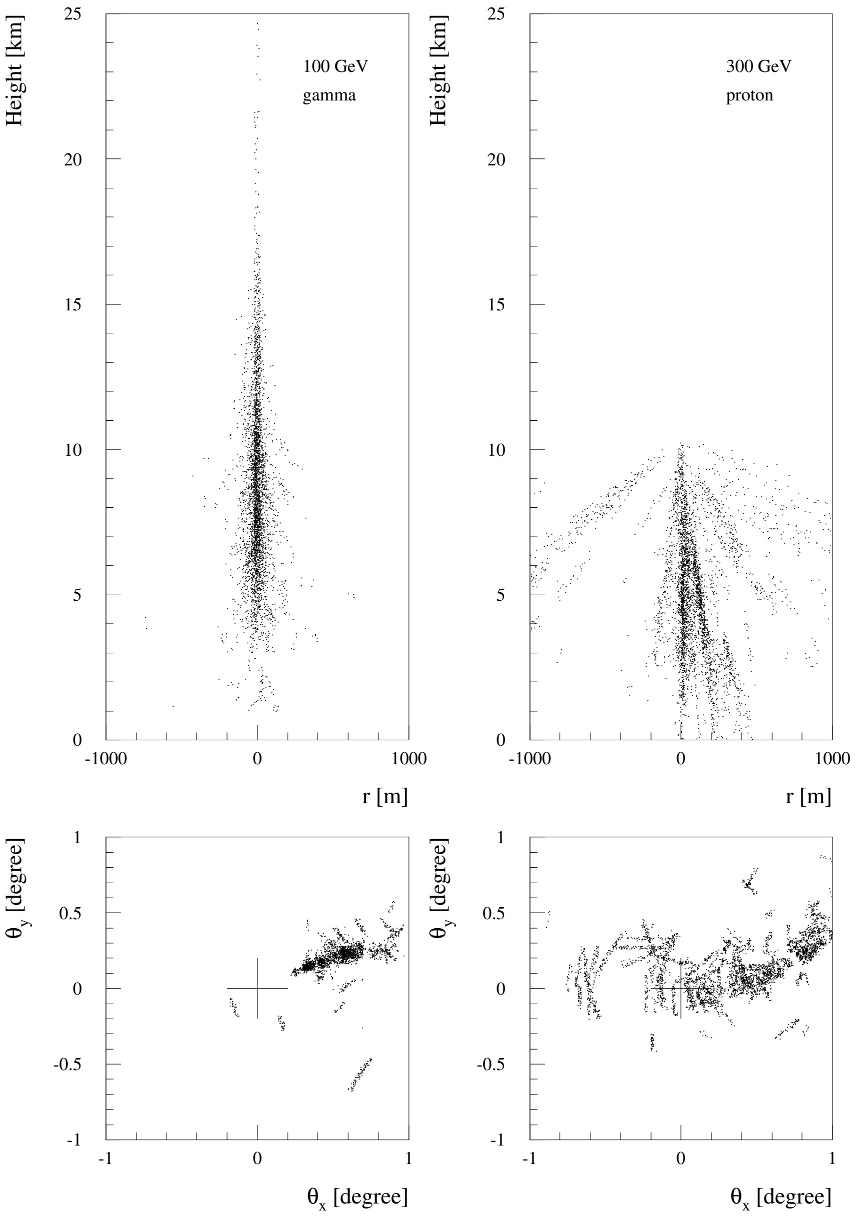

Figure 16. Longitudinal development of γ-ray and proton-induced showers and their images in the focal plane of the telescope.

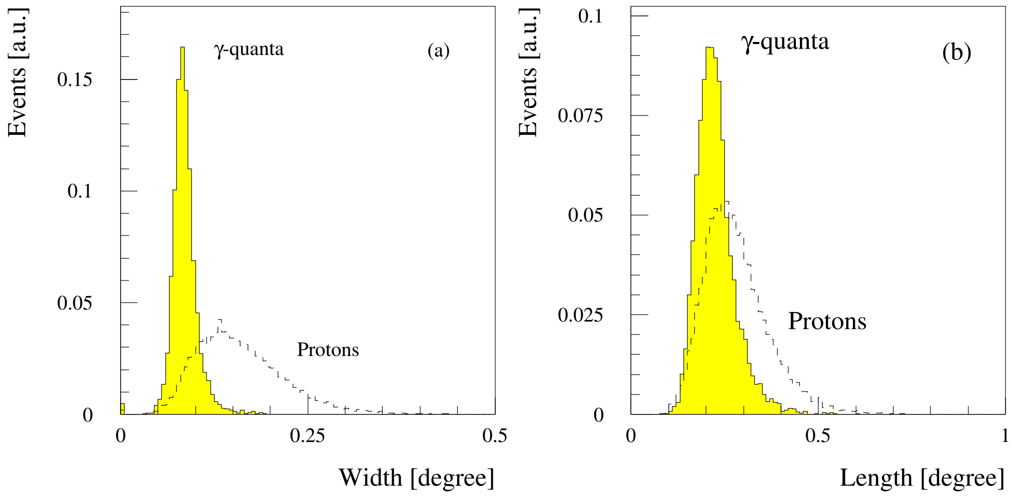

Figure 17. Distributions of the image 'shape' parameters **W**idth and **L**ength.

nal enhancement Q-factor of about 7 [36]. Note that similar ideas of using information contained in the positions of centroids of images detected by $\geq$ 2 telescopes are also discussed, in somewhat different formulations, in several recent papers [5,13,37,38]. Although the efficiency of this method is rather high, it appears less than the efficiency of the straightforward method based on the shower selection using the reconstructed arrival directions of individual showers. However, this method could be rather useful, in particular in cases when the determination of the image orientation with high precision is not possible, e.g. due to a low optical quality of the mirror, relatively large pixel size, steering problems with mounts, etc.

6.2. Suppression of the CR background based on the image shape information

After selection of events on the basis of event-by-event reconstruction of the shower directions, the further improvement of the γ-ray signal may be achieved by separation of the CR and γ-ray induced showers due to noticeable differences between their characteristics, caused by the large transverse momenta of the secondary hadrons, the deeper penetration of the hadronic cascades into the atmosphere, and the essential fluctuations in the hadronic cascades. These features are transferred effectively to the properties of the Cherenkov radiation, in particular to the angular distribution of the Cherenkov images (see Fig. 16). The Cherenkov images of the γ-ray showers have a compact shape and regular structure, in contrast to the rather diffuse and chaotic images from the CR background showers.

The distributions of the shape parameters **W**idth and **L**ength for a single telescope are shown in Fig. 17. The CR background rejection factors for the **W**idth and **L**ength cuts which provide $\kappa_\gamma = 0.8$ acceptance for γ-ray showers, for the camera with pixel size $0.25°$, $\kappa_{\rm p}^{-1} \simeq 7$ and 4, respectively (see Table 3). Note that these two parameters strongly correlate with each other. Therefore, after implementation of the **W**idth cut, the latter being the most effective shape parameter, the **L**ength cut somewhat improves the signal-to-noise ratio, but the enhancement is not very significant (see Table 3). Note also that the 'orientational' **A**lpha parameter provides approximately the same improvement factor for the γ-ray signal, $Q = \kappa_\gamma/(\kappa_{cr})^{1/2}$, as the 'shape' **W**idth and **L**ength parameters.

It should be noted that the distributions of the shape parameters as well as their average values depend on the configuration of the camera, in particular on the pixel size. However, for the pixel size $\leq 0.25°$ the instrumental distortion of im-

Table 3
The efficiency of the CR background rejection for a single IACT using the 'shape' **W**idth and **L**ength and 'orientational' **A**lpha parameters. The results are obtained for the same two configurations of the camera as in Table 2.

Camera:	Parameter:	κ_γ	κ_{cr}	Q-factor
(1)	**W**idth	0.804	0.152	2.06
	Length	0.806	0.253	1.60
	Length+**W**idth	0.775	0.136	2.10
	Alpha	0.563	0.058	2.34
(2)	**W**idth	0.791	0.133	2.16
	Length	0.804	0.216	1.73
	Alpha	0.572	0.052	2.51

Table 4
The CR background rejection efficiency of the IACT 'cell' using the image "shape" parameter **W**idth with and without "scaling" on the impact distance and energy of the primary particle. In the analysis the N-fold **W**idth cut (N = 2,3,4 where N is the number of the images passed the cut) was used.

Parameter:	Scaling:		2	3	4
Width	No	κ_γ	0.792	0.585	0.489
		κ_{cr}	0.116	0.038	0.016
		Q-factor	2.32	3.00	3.87
Width	Yes	κ_γ	0.891	0.634	0.490
		κ_{cr}	0.076	0.017	0.0036
		Q-factor	3.23	4.86	8.33

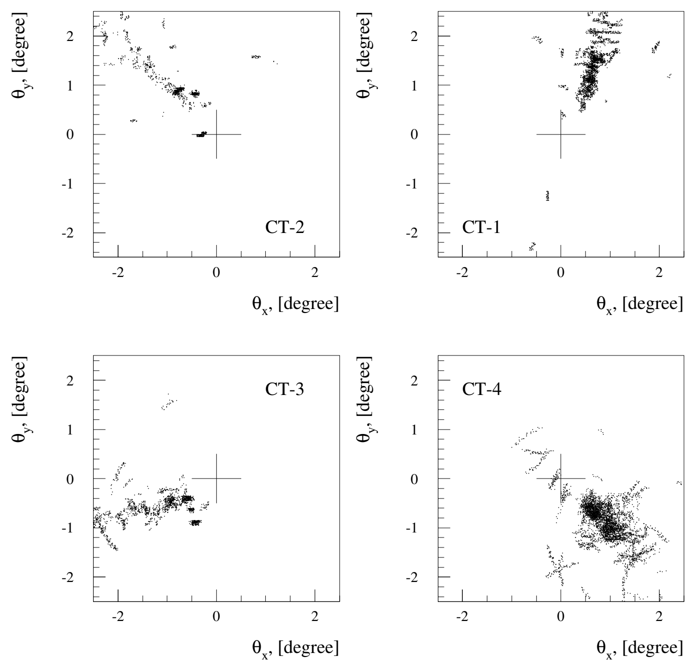

Figure 18. The Cherenkov light images in the focal planes of 4 IACTs of the 'cell' from a 500 GeV vertical proton-induced shower crossing the center of the 'cell'.

ages induced by the camera due to its finite granularity becomes less important (at least in the second-moment approach of the image parametrization) than the fluctuations of the image parameters caused by the stochastic development of air showers themselves [19]. Correspondingly the rejection efficiency of the CR background, based on the image shape analysis, is insensitive to the pixel size, provided that the latter is $\leq 0.25°$. Thus even with an ideal camera with infinitely small pixel size the Q-factors for a single telescope presented in Table 3 cannot be noticeably improved.

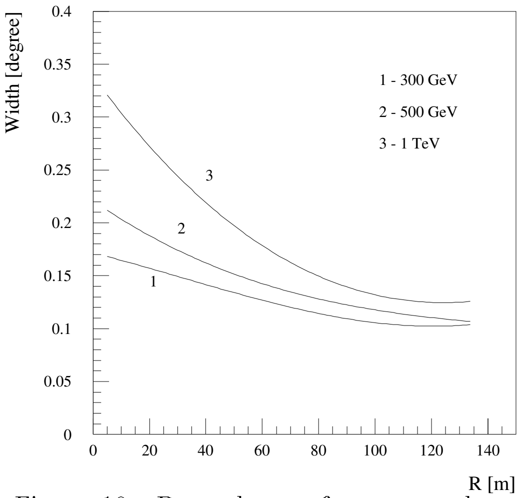

Figure 19. Dependence of average value of the **W**idth parameter of γ-ray showers on the impact distance to the IACTs.

Dramatic improvement of the Q-factors can be reached using the information about the shower images detected simultaneously by ≥ 2 IACTs, two principal reasons being responsible:

1. Although obviously the shower images in different projections are not independent, the correlation between the images detected by different separated telescopes is far from the 100 %. This is illustrated in Fig. 18 where an example of the shower induced by a 500 GeV proton seen by 4 IACTs of the 'cell' is shown. Since it is assumed that the arrival direction of the primary proton is parallel to the telescope axes, the reconstructed direction coincides nearly with the direction to the γ-ray source, thus this event 'passes' the 'γ-ray' cut. Moreover the images in one of the telescopes (CT-2) and also, to some extent, in CT-3 look like images produced by γ-rays. However, the images in CT-1, and especially in CT-4 are distinguishable as 'proton-images'. Therefore, with images registered in at least 3 telescopes one may sort out that event from the γ-ray sample. Thus, we may conclude that the analysis of *partially* correlated images should significantly improve the γ/proton separation power. The results of the analysis are shown in Table 4 where it is seen that the CR rejection power increases noticeably with increasing the IACT multiplicity.

2. For the given image tail cut, the image shape parameters depend strongly on the distance of the shower core R and the primary photon energy E_0 (see Fig. 19). This implies that each interval of E_0 and R has its own optimal 'cuts' separating the proton and γ-ray domains. Actually, the image detected by one telescope, namely its **D**istance and **S**ize parameters, contain some information about E_0 and R, but this information is averaged statistically, and does not concern the individual events. As a result, the chosen average 'cuts' work effectively only in certain narrow energy intervals, thereby noticeably reducing the effective dynamical range of the image analysis. The stereoscopic reconstruction of the shower core parameters allows to choose the image 'cuts' in different E_0 and R intervals. Therefore the 'correction' of the image parameters by the function $\lambda(R, E)$ softens the *energy- and distance*-dependence of the shape parameters and makes the CR and γ-ray domains more distinguishable. The scaling functions can be calculated for both the CR and γ-ray showers using Monte Carlo simulations. However, in practice we can use only 1 of these 2 functions corresponding to CR or γ-ray showers. Indeed, at the *first* stage of the image analysis the energy of the shower cannot be determined with an accuracy better than a factor of 2 (see Fig. 13), since the type of the primary particle *a priori* is not known. Under these circumstances one may apply the scaling function $\lambda_\gamma(R, E)$ calcu-

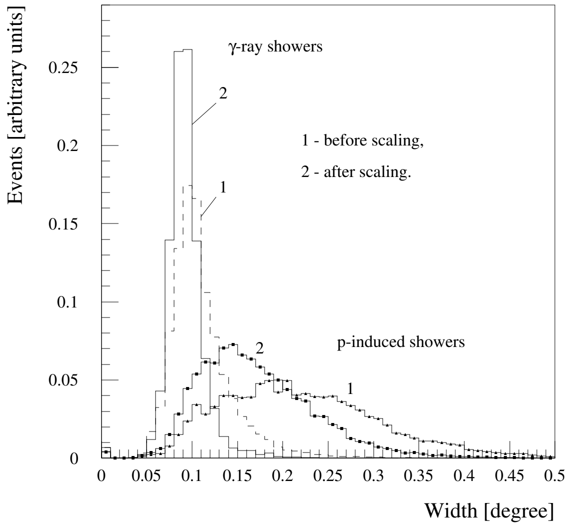

Figure 20. Distributions of the **W**idth parameter of γ-ray- and proton-induced showers detected by all 4 IACTs of the 'cell' with and without scaling procedure by a factor $\lambda(r, E)$.

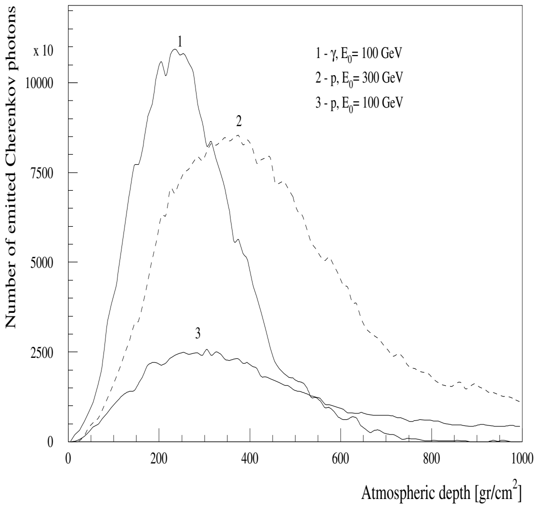

Figure 21. The number of emitted Cherenkov light photons from γ- and proton-induced showers at different depthes of the cascade development in the Earth's atmosphere.

lated for γ-ray showers, to both the γ-ray and CR data sets. The details of calculation of this function will be discussed elsewhere. Although this function, tuned to γ-rays, does not properly re-distribute the CR-induced showers, nevertheless it makes the separation of the **W**idth-distributions of γ-ray and CR showers noticeably better (see Fig. 20). For example, for the master mode of 4 IACTs in coincidence the scaling function results in an increase of the CR rejection factor from 62 to 250. Note that the **W**idth cut used in Table 4 for the multi-telescope analysis is different (larger) than the optimum cut used in Table 3 for a single telescope. The reason was to keep a $\geq 50\%$ γ-ray acceptance after multiple application of the cuts to the shower images in different projections.

Above we have discussed the efficiency of γ/proton separation based only on the application of the **W**idth parameter for γ/proton separation. The other parameters, being less effective, nevertheless improve somewhat the CR rejection power when they are applied separately. However, as it was argued above for the single IACT, the joint application of the **W**idth and **L**ength cuts does not essentially improve the CR background rejection. This is true, to greater extent, for the system of IACTs. The reduction of the CR background by a factor of several hundreds using only **W**idth cuts in different projections does not leave room for the further enhancement of the γ-ray signal.

6.3. Other approaches

1. *Position of the shower maximum.* The position of the image centroid in the focal plane which is characterized by the **D**istance parameter indicates the direction to the region in the atmosphere where the maximum amount of the Cherenkov light is produced. The stereoscopic detection of the shower allows, by intersection of at least two vectors starting from each telescope, the position of the shower maximum in space (see Fig. 8) to be found. Since the longitudinal development of the γ-ray and proton induce cascades are different (see Fig. 21), the height of the shower max-

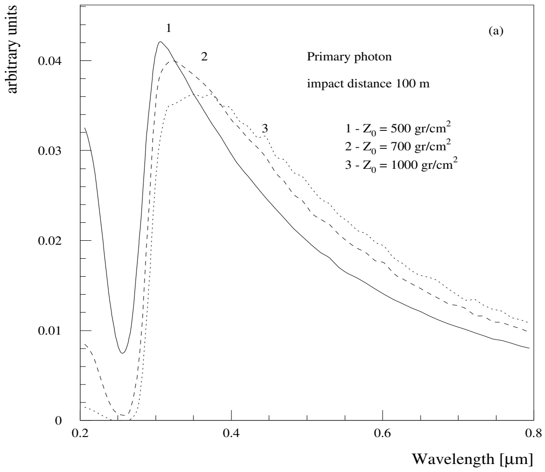

Figure 22. The spectra of the Cherenkov radiation from γ-ray and proton-induced showers at different observation levels.

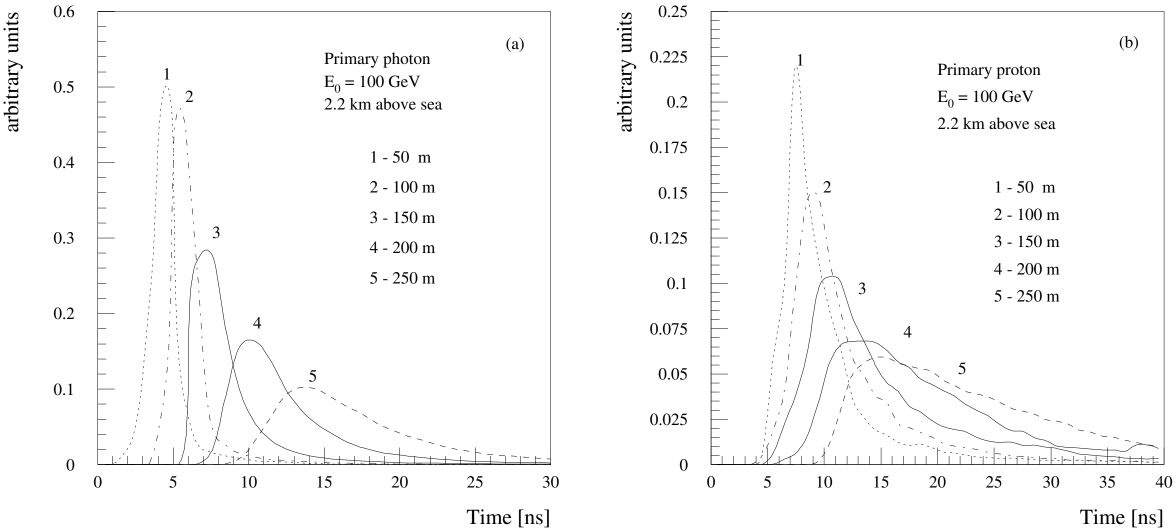

Figure 23. The Cherenkov light time impulses from γ-ray and proton-induced showers at the different distances from the shower core.

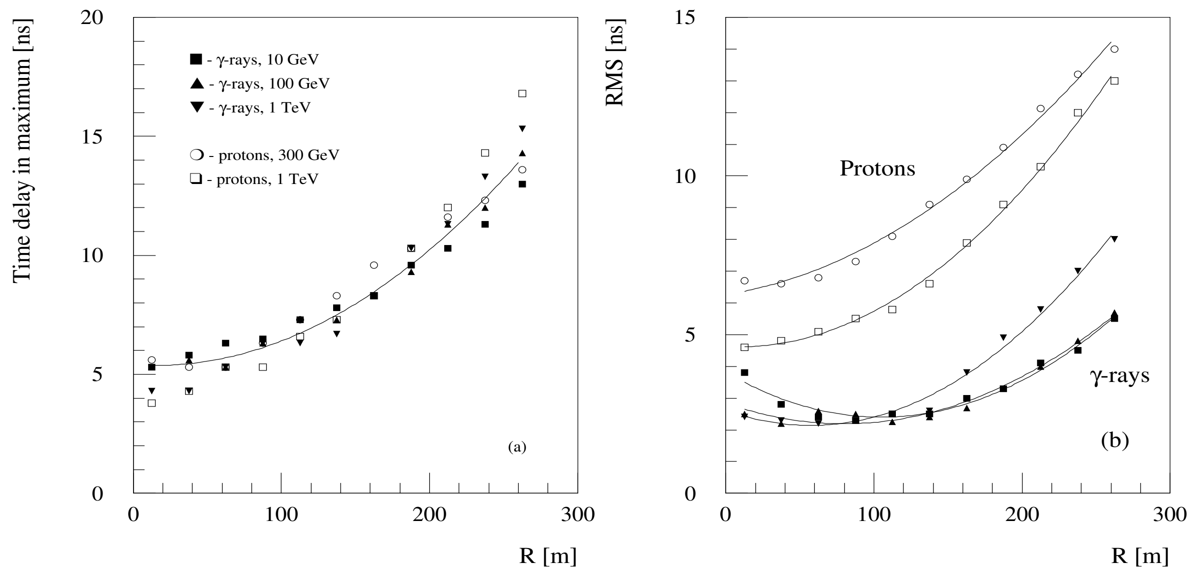

Figure 24. The average curvature and the fluctuations of the time front of the Cherenkov light pool from γ-ray and proton-induced showers at sea level.

imum $H_{\max}$ contains a certain information about the nature of the primary particle. Therefore, one may hope that the *direct* determination of the height of the shower maximum $H_{\max}$ can provide a noticeable suppression of the CR induced events. The error in the determination of $H_{\max}$ depends on the accuracy of the **D**istance parameter. In particular, an error in the image centroid position of $\approx 0.1°$ results in ≈ 1 km uncertainty in $H_{\max}$. The Monte Carlo calculations show that the standard deviation of the $H_{\max}$ determined by 4 IACTs of the 'cell' is about of 1.2, 1.0, 0.8 km at energies of γ-rays 300 GeV, 1 TeV, 3 TeV, respectively. The improved accuracy at larger energies is due the better statistics of the photoelectrons in the image. Unfortunately, the 1 km uncertainty in determination of $H_{\max}$ as well as a strong overlap of the longitudinal distributions of the γ-ray and proton showers (see Fig. 21) do not allow one to use information about $H_{\max}$ for an effective rejection of the CR background. The Monte Carlo calculations show that the γ-ray signal improvement (Q-factor) does not exceed a factor of 1.5. Moreover, note that $H_{\max}$ enters *indirectly* into the image shape parameters. For example, the **W**idth of the image is determined not only by the angular distribution of the secondary cascade particles, but also by the distance from the telescope to the particles emitting the Cherenkov light. Therefore the information about the primaries contained in $H_{\max}$ is partially used already in the image shape analysis. Thus, the use of $H_{\max}$ for the selection of γ-ray showers does not seem to be practicable, especially after the image shape analysis.

2. UV-*content.* The difference in the longitudinal development of γ-ray and proton induced showers is reflected, to some extent, in the spectrum of the Cherenkov radiation. Due to deeper penetration of the hadronic showers the Cherenkov light of the latter contains a noticeable amount of UV photons, especially at high altitudes, in contrast to the Cherenkov radiation of γ-ray showers which shows a sharp cutoff at wavelengths below 300 nm caused by the light absorption and scattering in the atmosphere. It

is demonstrated in Fig. 22. Grindlay [39] and Stepanian et al. [40] have proposed to use the difference in UV-content in γ-ray and proton showers for suppression of the CR background. Although the expected signal-to-noise enhancement factor based on the independent 'UV content' analysis is estimated $Q_{\rm UV} \sim 2$ [40], the method seems to be not very effective after the filtering of the showers through the image shape 'cuts' since the image shape parameters correlate significantly with the 'UV/visible' ratio [41].

3. *Timing.* The temporal characteristics of the Cherenkov light of the air showers provide an *independent* method to determine the shower arrival direction, and distinguish, at the certain level, the γ-ray and proton primaries. Determination of the shower direction is based on the differences in the photon arrival times at the observational level.

The time-structure of the Cherenkov light contains combined information about the lateral, longitudinal, and angular distribution of the cascade particles. Therefore it can be used, in principle, for identification of the primary particles. The temporal distributions of the Cherenkov light from γ-ray and proton showers with different impact parameters are shown in Fig. 23. It is seen that time-spectra of γ-ray showers are narrower with smooth shape, while the distributions of the proton showers are broader and structured. However due to a significant overlap of the distributions of γ-ray and proton shower Cherenkov light pulses the use of the reconstructed time fronts is not effective. This can be seen in Fig. 24a where average photon arrival times for protons and γ-ray showers are shown; independent of the type and energy of primaries the average front curvatures are very similar. Much more effective is the method based on the differences in the fluctuations of the pulses from γ-ray and proton showers [42]. The RMS of the time pulses are shown in Fig. 24b for 2 different primary energies, 100 GeV and 300 GeV. The significant differences between γ-ray and proton showers indicate that the fluctuations in the pulse duration *alone* provide the signal enhancement Q-factor of about 3-4. However, the calculations also show that this technique becomes significantly less efficient ($Q \to 1$) when being applied to the events which have already passed the image shape cuts.

7. Summary

It is generaly accepted that the imaging atmospheric Cherenkov technique is the most effective and convincing approach in VHE γ-ray astronomy at energies between 100 GeV and 10 TeV. The current results obtained by several *mono* IACTs (Whipple, HEGRA, CANGAROO) encourage an optimistic view for the future of the field. A further qualitative improvement of the IACT technique is to be expected for the *stereoscopic* measurement of showers by several IACTs in a system. In this paper we have discussed the capabilities of four '100 GeV' class IACTs located in the corners of the 100 m × 100 m quadrangle, which may be recommended as a possible basic 'cell' for future telescope arrays containing $\gg 10$ IACTs.

In calculations we have assumed that the 'cell' of telescopes with aperture in respect to the number of photoelectrons $S_{\rm ph.e.} = S_{\rm m} \cdot \chi_{\rm ph \to e} = 10\,{\rm m}^2$ is located at 2.2 km a.s.l. We have analyzed two different designs for the imaging camera, a 271-channel camera with pixel size 0.25° (FoV=4.75°) and a 469-channel camera with pixel size 0.15° (FoV=3.75°). Our study shows that although the small pixel size ($< 0.25°$) cameras may have an advantage when they are used in *mono* IACTs, in the case of operation in the *stereoscopic* mode, a reduction of the camera's granularity below 0.25° does not lead to noticeable improvements of the accuracy of determination of shower characteristics, at least in the standard second-moment image parametrization approach. Thus we conclude that use in future multi-telescope systems relatively economical cameras with pixel-size $\approx 0.25°$ and relatively large FoV$\approx 5°$, will be quite sufficient for a proper study of the primary γ-radiation.

The principal conclusion of this study may be formulated as follows:

1. The 100 m × 100 m 'cell' of IACTs provides high detection efficiency of γ-ray showers ($\to$ 100% at $E \geq 200\,{\rm GeV}$), with cores inside the 'cell', where a coincidence of all four telescopes

is required. The lower detection efficiency of CR-induced showers results in strong separation of the energy domains of detected γ-rays and CR protons, with a maximum of differential detection rates at $\sim$ 100 GeV and $\sim$ 1 TeV, respectively. This provides suppression of the hadronic showers by a factor of 10 already at the hardware (trigger) level.

2. The 'cell' operating in the '4-fold IACT coincidence' mode allows to measure the arrival direction of individual showers with angular resolution, corresponding to 68% acceptance of γ-ray events, of $\delta\theta = 0.1°$, $0.075°$ and $0.05°$ for E=100 GeV; 300 GeV, and 1 TeV, respectively.

3. Since the showers detected by all 4 IACTs are located at distances of about $\sim$ 100 m from at least 2 telescopes, the fluctuations of the Cherenkov light density appear small enough to determine the energy of γ-ray showers with an accuracy of $\leq 20\%$.

4. The reconstruction of the shower arrival directions by the IACT 'cell' on an *event-by-event* basis with accuracy $\leq 0.1°$ provides very effective reduction of the CR background contamination. In particular, for γ-ray point sources the contribution of the CR events detected within the trigger region $\approx 3°$ can be reduced by a factor of several hundred. Thus the directional information alone already results in significant enhancement of the signal-to-noise ratio by a factor of $Q^{(\mathrm{dir})} \sim 10$. After selection of events by their directions, a further strong improvement of the signal by a factor of $Q^{(\mathrm{shape})} \geq 8$ may be achieved by the rejection of the CR background due to the differences (in shape and intensity) of Cherenkov light images of hadronic and electromagnetic showers detected simultaneously by 4 IACTs of the 'cell', when only one in 300 events passes the cuts.

The very effective γ/proton separation by directional and shape criteria allows almost 'background-free' detection of γ-ray point sources with flux $J_\gamma(\geq 100\,\mathrm{GeV}) = 10^{-11}\ \mathrm{cm}^{-2}\mathrm{s}^{-1}$ ($\leq \frac{1}{10}$ flux of the Crab), as well as the study of moderately extended diffuse γ-ray sources with angular size $\sim 1°$. The minimum detectable fluxes of γ-rays depend on the observational time and the detection area of showers, i.e. the number of 'cells' in the IACT array.

The flux sensitivities of such arrays as well as their ability for angular and spectroscopic measurements are discussed in the companion paper.

Acknowlegments

We would like to thank A.V. Plyasheshnikov for many fruitful discussions.

REFERENCES

1. C.E. Fichtel et al., Ap. J. Suppl. 90 (1994) 917.
2. D.J. Thompson et al., Ap. J. Suppl. 101 (1995) 259.
3. J.W. Cronin, K.G. Gibbs and T.C. Weekes, Ann. Rev. Nucl. Part.Sci. 43 (1993) 883.
4. M.F. Cawley and T.C. Weekes, Exp. Astron. 6 (1996) 7.
5. A.M. Hillas, Space Sci. Rev. 75 (1996) 17.
6. R.C. Lamb, Space Sci. Rev. 75 (1996) 53.
7. R.C. Lamb, C.E. Covault and R.A. Ong, The University of Chicago, preprint EFI 95-14 (1995).
8. R.A. Ong, D. Bhattacharya, C.E. Covault et al., in: Proc. Towards a Major Atmospheric Cherenkov Detector IV, ed. M. Cresti (Padova, 1995) p. 261.
9. T. Tanimori, K. Sakurazawa, T. Tsukagoshi, K. Ohasaki and T. Kifune, in: Proc. Towards a Major Atmospheric Cherenkov Detector III, ed. T. Kifune (Tokyo, 1994) p. 311.
10. S.M. Bradbury, J. Busch, E. Feigl et al., in: Proc. Towards a Major Atmospheric Cherenkov Detector IV, ed. M. Cresti (Padova, 1995) p. 277.
11. F.A. Aharonian, in: Proc. Towards a Major Atmospheric Cherenkov Detector III, ed. T. Kifune (Tokyo, 1994) p. 227.
12. A.M. Hillas, Proc. 19th ICRC, La Jolla, 3 (1985) p. 445.
13. P.M. Chadwick, J.E. Dickinson, M.R. Dickinson et al., Space Sci. Rev. 75 (1995) 153.
14. F.A. Aharonian et al., in: Proc. Towards a Major Atmospheric Cherenkov Detector II, ed. R.C. Lamb (Calgary, 1993) p. 81.
15. M. Teshima et al., in: Proc. Tokyo Workshop on Techniques for the Study of Extremely High Energy Cosmic Rays, ed. M. Nagano (Tokyo, 1993) p. 109.
16. T.C. Weekes et al., Proposal (internal report) (1995).
17. W. Hofmann and C. Köhler, in preparation (1997).

18. C. Köhler, G. Hermann, W. Hofmann, A. Konopelko and A. Plyasheshnikov, Astropart. Phys., (1996).
19. F.A. Aharonian, A. Heusler, W. Hofmann et al., J. Phys. G: Nucl. Part. Phys. 21 (1995) 985.
20. M. Panter et al., Proc. 22nd ICRC, Rome, 1 (1995) p. 958.
21. M.F. Cawley et al., Exp. Astron. 1 (1990) 173.
22. R. Mirzoyan, V. Fomin, A. Stepanian, Nucl. Instrum. Methods A 373 (1995) 153.
23. A.K. Konopelko, A.V. Plyasheshnikov and A.A. Schmidt, Preprint No. 6, Moscow Lebedev Physical Institute (1992).
24. L. Elterman, Preprint AFC RL-68-153, Air Force Cambridge Res. Lab. (1968).
25. S. Sinha, J. Phys. G: Nucl. Part. Phys. 21 (1995) 473.
26. A.M. Hillas, MOCCA simulations, private communication.
27. Y.M. Shabelsky, Nucl. Phys. 45 (1987) 223.
28. J. Ranft and J.T. Routti, Particle Accelerators 4 (1972) 11.
29. A.M. Hillas, Proc. 16th ICRC, Kyoto, 6 (1979) 13.
30. J. Capdeville et al., Preprint KfK-4998, Karlsruhe Kernforschungszentrum (1992).
31. A.V. Plyasheshnikov, F.A. Aharonian, W. Hofmann et al., in preparation (1997).
32. F.A. Aharonian, W. Hofmann, A.K. Konopelko et al., J. Phys. G: Nucl. Part. Phys. 21 (1995) 985.
33. B. Wiebel, 1994, Preprint WUB 94-08, Univ. of Wuppertal (1994).
34. D.J. Fegan, Space Sci. Rev. 75 (1996) 137.
35. R.M.L. Baker and M.W. Makemson, An Introduction to Astrodynamics (Academic Press, New York, 1967).
36. A.K. Konopelko, in: Proc. Towards a Major Atmospheric Cherenkov Detector IV, ed. M. Cresti (Padova, 1995) p. 373.
37. A.A. Stepanian, Nuclear Physics B (Proc. Suppl.) 39A (1995) 207.
38. F. Krennrich and R.C. Lamb, Exp. Astron. 6 (1995) 285.
39. J.E. Grindlay, Nuovo Cimento 2B (1971) 112.
40. A.A. Stepanian, V.P. Fomin and B.M. Vladimirsky, Bull. Crimea Astophysics Observatory 66 (1983) 234.
41. F.A. Aharonian, A.A. Chilingarian, A.K. Konopelko and A.V. Plyasheshnikov, Nucl. Instrum. Methods A 302 (1991) 522.
42. A.K. Konopelko, A.V. Plyasheshnikov and A.A. Shmidt, Proc. of 22nd ICRC, Dublin, 1 (1991) 484.